CrossMark

The "Tsunami Earthquake" of 13 April 1923 in Northern Kamchatka: Seismological and Hydrodynamic Investigations

Amir Salaree[1] and Emile A. Okal[1]

Abstract—We present a seismological and hydrodynamic investigation of the earthquake of 13 April 1923 at Ust'-Kamchatsk, Northern Kamchatka, which generated a more powerful and damaging tsunami than the larger event of 03 February 1923, thus qualifying as a so-called "tsunami earthquake". On the basis of modern relocations, we suggest that it took place outside the fault area of the mainshock, across the oblique Pacific-North America plate boundary, a model confirmed by a limited dataset of mantle waves, which also confirms the slow nature of the source, characteristic of tsunami earthquakes. However, numerical simulations for a number of legitimate seismic models fail to reproduce the sharply peaked distribution of tsunami wave amplitudes reported in the literature. By contrast, we can reproduce the distribution of reported wave amplitudes using an underwater landslide as a source of the tsunami, itself triggered by the earthquake inside the Kamchatskiy Bight.

Key words: Tsunami, Kamchatka, landslides, simulations.

1. Introduction

In the Winter and Spring of 1923, the eastern coast of Kamchatka was the site of a series of major earthquakes, two of which generated devastating tsunamis. Their effects, investigated in detail in the years following the events by Troshin and Diagilev (1926) and later Meniaĭlov (1946) were summarized by Soloviev and Ferchev (1961). The main shock (hereafter MS) occurred on 03 February 1923 at 16:01 GMT, (03:01 local time on the 4th), in a very sparsely populated area along the Kronotskiy Bight (Fig. 1). It provoked serious damage both in Petropavlovsk-Kamchatskiy to the south, and Ust'-Kamchatsk in the north, and was followed by a powerful tsunami reaching run-up heights of 6 m, which washed away a warehouse at Ust'-Kamchatsk (Soloviev and Ferchev 1961). Incidentally, the tsunami motivated what is believed to be the first far-field warning by Jaggar (1930) at the Hawaii Volcano Observatory, which unfortunately was not heeded, leading to considerable damage and one casualty on the Island of Hawaii (Okal 2011).

Among its numerous aftershocks, the event of 13 April (O.T. 15:31 GMT) near Ust'-Kamchatsk (hereafter the UK event) stands out as featuring properties typical of a "tsunami earthquake". We recall that the name *tsunami earthquake* was introduced by Kanamori (1972) to characterize events whose tsunami is significantly larger than expected from their seismic magnitudes, especially conventional ones. Fukao (1979) and later Tanioka et al. (1997) and Polet and Kanamori (2000) have explained their properties as due to anomalously slow rupture along the fault, resulting in red-shifting of the seismic spectrum towards lower frequencies. Another, mechanically different, scenario can involve the triggering by the earthquake of a major underwater landslide, which can act as ancillary tsunami generator, a classical example being the Papua New Guinea disaster of 17 July 1998 (Synolakis et al. 2002); these are not generally considered "tsunami earthquakes". The catastrophic 1946 Aleutian tsunami is believed to have featured both an anomalously slow seismic source, and a locally devastating landslide (Okal et al. 2003; López and Okal 2006).

As hinted by the traditional magnitudes ("M_{PAS}") assigned by Gutenberg and Richter (1954) to the MS (8.4) and UK (7.2) events, the latter is clearly a smaller source from a seismological standpoint. In

[1] Department of Earth and Planetary Sciences, Northwestern University, Evanston, IL 60208, USA. E-mail: amir@earth.northwestern.edu; emile@earth.northwestern.edu
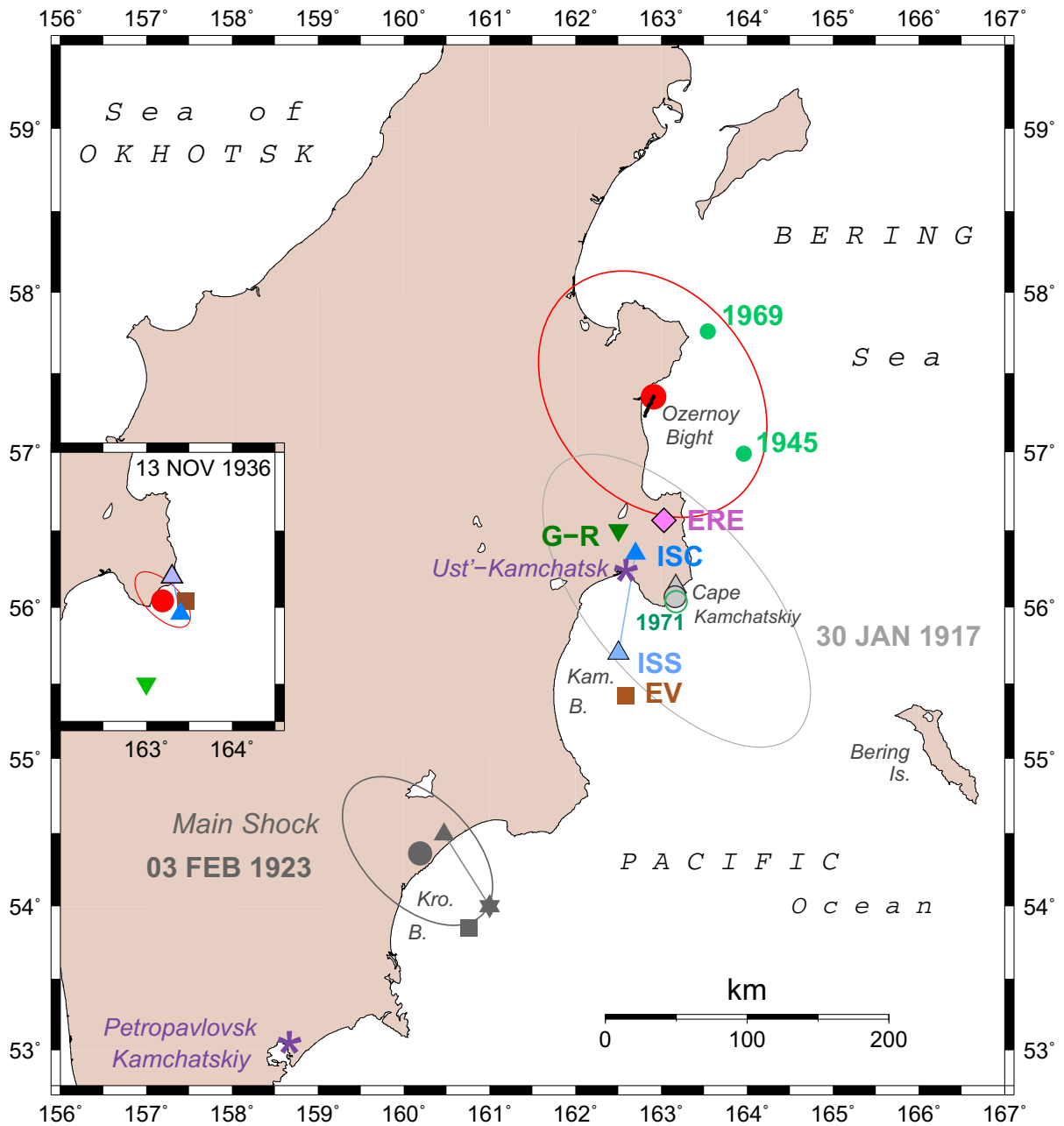
Figure 1
Relocation of the 1923 Ust'-Kamchatsk earthquake. Our preferred relocation is shown as the red dot, with associated Monte-Carlo ellipse, and small black dots identifying the negligible moveout of the epicenter as a function of constrained depth; the triangles are the initial ISS location (light gray) and the recent ISC relocation (in blue); the inverted green triangle is Gutenberg and Richter's (1954) solution, the brown square Engdahl and Villaseñor's (2002) Centennial Catalog epicenter, and the magenta diamond E.R. Engdahl's recent solution (pers. comm., 2017). For reference, we show epicentral estimates for the 1923 main shock (in dark gray with the same symbols), and for the 1917 event at Cape Kamchatskiy (in light gray). Also shown are the epicenters of the events at Ozernoy (1945 and 1969; solid green dots) and Cape Kamchatskiy (1971; open green dot). Kam. B.: Kamchatskiy Bight; Kro. B.: Kronotskiy Bight. To avoid clutter, the results for the 1936 Cape Kamchatskiy event are shown in the inset at left, on the same scale and with the same symbols as for the UK earthquake, but displaced 6° in longitude. Note the total identity of the 1917, 1936 and 1971 epicenters

Ust'-Kamchatsk, it caused only marginally more damage than the main shock, despite a clearly shorter epicentral distance. Yet, the tsunami from the UK event was significantly stronger than that of the mainshock. It ran up 11 m at Ust'-Kamchatsk, killing at least 23 people and totally destroying several canneries and other infrastructure. According to Zayakin and Luchinina (1987), the maximum run-up (20–30 m) took place in the vicinity of the First Creek ("Pervaya Rechka"), and of the cannery Nichiro which was completely destroyed, one of its cutters being deposited on a terrace 20 m high and 1 km inland. This location is estimated to be 27 km WSW of Ust'-Kamchatsk (note that their Fig. 3.10.2, p. 20, like all others, bears no scale). Inundation distances reached 7 km along the river valley at the mouths of the Kamchatka River.

It is worth noting that no mention is made of a tsunami following the aftershock on 24 February 1923 (A12 in Table 1), to which Gutenberg and Richter (1954) assigned a larger magnitude ($M_{PAS} = 7.4$) than to the UK event, thus supporting

the anomalous character of the latter. In this respect, the sequence of 1923 Kamchatka events is comparable to the 1932 Mexican series (Okal and Borrero 2011): a mainshock with a significant tsunami (03 February 1923/03 June 1932), a strongest aftershock without a tsunami (24 February 1923/18 June 1932), and a very powerful tsunami during a clearly smaller aftershock (13 April 1923/22 June 1932), the latter being a typical tsunami earthquake.

These remarks motivate a detailed seismological and hydrodynamic reassessment of the UK event of 13 April 1923, which is the subject of this paper.

2. Relocation

We relocated the 1923 Kamchatka sequence, starting with the foreshocks of 02 February, and including all regional activity for the 6 months following the main shock. We used arrival times listed in the International Seismological Summary (ISS) and the iterative, interactive technique of Wysession

Table 1

Relocations performed in this study

No.	Date	Time (GMT)	Epicenter (°N)	(°E)	Depth (km)	Stations Read	Used	r.m.s. (s)	Magnitude
			1923 series						
F1	02 FEB (033) 1923	01:06:40.6	53.99	161.60	10	29	22	3.74	6.7 ISC
F2	02 FEB (033) 1923	05:07:41.0	54.13	160.88	10	54	45	4.71	7.2 PAS
M3	**03 FEB (034) 1923**	**16:01:47.9**	**54.36**	**160.19**	**10**	**79**	**66**	**4.51**	**8.4 PAS**
A4	03 FEB (034) 1923	17:40:59.1	53.85	162.99	10	9	7	5.06	
A5	03 FEB (034) 1923	18:42:56.8	53.26	160.76	10	27	26	4.20	
A6	03 FEB (034) 1923	18:50:46.8	54.17	163.88	10	11	10	3.60	
A7	05 FEB (036) 1923	22:23:34.8	54.07	161.70	10	8	8	3.54	
A8	11 FEB (042) 1923	22:45:54.9	55.76	161.21	103[a]	16	16	3.37	6.2 ISC
A9	12 FEB (043) 1923	01:58:41.7	54.58	162.10	10	30	25	3.65	6.4 ISC
A10	15 FEB (046) 1923	22:40:36.8	51.24	150.05	433[a]	4	4	–	
A11	18 FEB (049) 1923	23:39:54.3	56.31	161.03	21[b]	9	7	2.44	
A12	24 FEB (055) 1923	07:34:40.8	55.58	162.54	10	52	45	4.71	7.4 PAS
UK13	**13 APR (103) 1923**	**15:31:06.3**	**57.35**	**162.91**	**10**	**40**	**31**	**3.34**	**7.2 PAS**
A14	23 MAY (143) 1923	22:37:08.3	53.83	161.09	10	45	34	3.96	6.4 ISC
			Other events						
	30 JAN (031) 1917	02:45:37.5	56.07	163.16	10	47	38	3.74	8.1 PAS
	13 NOV (318) 1936	12:31:30.0	56.04	163.19	10	207	198	3.14	7.2 PAS
	15 APR (105) 1945	02:35:30.2	56.99	163.96	69[a]	112	104	3.20	7.0 PAS

F foreshock, *M* mainshock, *A* aftershock, *UK* Tsunami earthquake

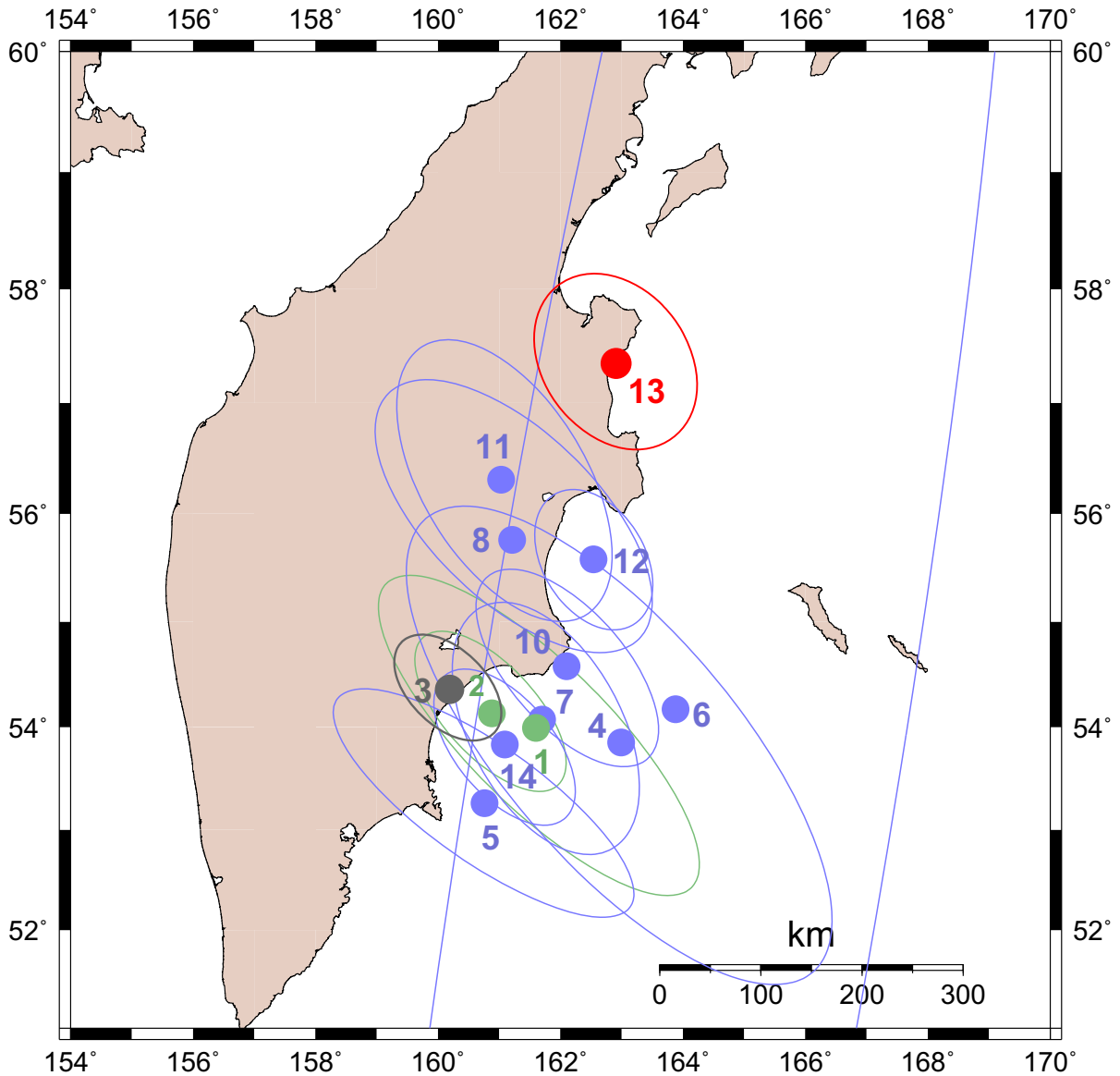[a]Floated depth: all other depths constrained

Figure 2
Relocation of the 1923 series. Individual events are shown with their numbers keyed to Table 1, and associated Monte Carlo ellipses. Foreshocks in green, Mainshock in dark gray, UK event in red. Event 10, relocating to the the Sea of Okhotsk slab, is not shown

et al. (1991), which includes a Monte Carlo algorithm injecting Gaussian noise into the dataset; for events in 1923, we use a standard deviation of the noise $\sigma_G = 8$ s. Results are listed in Table 1 and on Figs. 1 and 2. With the exception of events A8, A10 and A11, no floating depth relocations converged, and hypocentral depths were thus constrained to 10 km. We note that Event A10, initially proposed by the ISS at 55°N,

162.5°E, relocates to the Sea of Okhotsk slab, at a depth of 443 km; while the event is very poorly constrained (with only 4 arrival times), there is no reason to include it as part of the aftershock sequence, and we exclude it from Fig. 2.

As shown on Fig. 2, aftershocks A5, A14, A7, A10 and A12, reasonably well located with semi-minor axes of their Monte Carlo ellipses not

exceeding 50 km in the direction parallel to the trench, would suggest a rupture zone ~ 260 km long, to which Event A11 could also belong, and which also includes the two foreshocks (F1 and F2; shown in green on Fig. 2). We note that the largest aftershock (Event A12; $M_{PAS} = 7.4$) would, in this context, map at the edge of the fault zone, thus supporting the model proposed for smaller, intraplate earthquakes by Ebel and Chambers (2016). Event A8, relocating at a floated intermediate depth (103 km), may be triggered by stress transfer inside the slab. Events A4 and A6 are too poorly located to draw any conclusion.

Of particular interest is the relocation of the tsunami earthquake of 13 April 1923. The original ISS epicenter (55.7°N, 162.5°E) would fit at the end of the rupture area defined above, but the solution relocated as part of the GEM-ISC project (Storchak et al. 2015) moves inland, 18 km NNE from Ust'-Kamchatsk (56.36°N; 162.70°E), and only 20 km from Gutenberg and Richter's (1954) estimate ($56\frac{1}{2}$°N, $162\frac{1}{2}$°E; rounded off to the nearest 1/2°). By contrast, Engdahl and Villaseñor's (2002) location, part of their Centennial Catalogue, maps about 35 km south of the initial ISS epicenter, and more than 105 km from the revised ISC-GEM one. Our own solution, 57.35°N, 162.91°E, locates about 110 km north of the ISC-GEM epicenter, and its Monte Carlo ellipse encompasses most of Ozernoy Bight. Finally, a new solution by E.R. Engdahl (pers. comm., 2017) relocates to 56.56°N, 163.03°E, 30 km NNE of the GEM-ISC epicenter, and misses our ellipse by only 3 km. The disparity between modern relocations based a priori on the same dataset reflects its poor quality and probably results from the elimination of different sets of poor fits by various authors. Their choice remains to some extent subjective in interactive algorithms such as Wysession et al.'s (1991) where incompatible solutions are removed by the operator in an interactive process, and possibly inconsistent among fully automated ones. The situation is aggravated in the case of "tsunami earthquakes" by the slow nature of the source, which causes emergent arrivals in the near and far fields, with inconsistent picks on the part of different station operators, as described by Bell et al. (2014) in the case of the 1947 Hikurangi earthquakes in New Zealand. Finally, note

that relocation at a different constrained depth affects our epicenter only marginally (a total of 16 km between depths of 5 and 100 km; solid dots on Fig. 1).

The bottom line of these relocation efforts is that the UK event most probably occurred north of the rupture zone of the MS, being triggered by Coulomb stress to the vicinity of the triple junction near Cape Kamchatskiy, or even farther north, in the Ozernoy Bight, in the direction of the epicenter of the large earthquake of 22 November 1969 (57.76°N, 163.54°E; $M_S = 7.3$). That event was given a mostly strike-slip mechanism ($\phi = 46°$; $\delta = 71°$; $\lambda = 38°$) by Fedotov et al. (1973), but a low angle thrust one ($\phi = 225°$; $\delta = 16°$; $\lambda = 97°$) by Cormier (1975), for which the auxiliary plane is close to the strike-slip plane. As detailed in Sect. 4, it generated a substantial tsunami along Ozernoy Bight (Fedotov et al. 1973; Martin et al. 2008), but recorded in Ust'-Kamchatsk with an amplitude of only 20 cm.

Note that the area of Cape Kamchatskiy was the site of two major events, on 30 January 1917 and 15 December 1971, respectively. The latter ($M_S = 7.8$) is well located at 56.04°N, 163.17°E, and was studied by Gusev et al. (1975) and Okal and Talandier (1986). Its mechanism ($\phi = 276°$; $\delta = 21°$; $\lambda = 158°$) can be interpreted as predominantly strike-slip on a shallow dipping plate, expressing the extremely oblique subduction of the Pacific plate under the Bering Sea along the westernmost part of the Aleutian-Commander island chain. Okal and Talandier (1986) obtained a moment of 6×10^{27} dyn-cm from the modeling of surface waves at mantle periods. The earthquake generated a moderate tsunami, reaching an amplitude of 47 cm on the maregraph at Ust'-Kamchatsk (Gusev et al. 1975). The 1917 event was given a magnitude $M_{PAS} = 8.1$ by Gutenberg and Richter (1954). Modern relocation efforts (56.14°N, 163.17°E, ISC-GEM; 56.07°N, 163.16°E, this study) suggest a location identical to that of the 1971 event, but no tsunami was reported, despite the occurrence of the event in daylight (02:45 GMT or $\sim 13:38$ solar time). In addition, a smaller earthquake took place on 13 November 1936, which we relocated at essentially the same location (56.04°N; 163.19°E; inset on Fig. 1). This event was assigned $M_{PAS} = 7.2$ by Gutenberg and Richter

(1954). An instance of anomalous wave action was described following the 1936 shock, but it took place at night during stormy weather, leading Soloviev and Ferchev (1961) to doubt its interpretation as a tsunami. Figure 1 shows a total identity of epicenters for the 1917, 1936 and 1971 events.

Finally, we also examined the earthquake of 15 April 1945 ($M_{PAS} = 7.0$) which Bourgeois et al. (2006) proposed as the origin of tsunami deposits in the southern Ozernoy Bight. Even though the ISS entry mentions "Pasadena suggests deep focus", Gutenberg and Richter (1954) list it as shallow; a floating depth relocation does converge on (56.99°N, 163.96°E; 69 km), but the residual for constrained solutions is practically insensitive to hypocentral depth, and there is no reason to assume that the event is not shallow, especially given the absence of modern seismicity deeper than 50 km in the area.

In addition to the arrival times listed by the ISS and used in the various relocation efforts mentioned above, another constraint on the location of the UK event could be macroseismic data, i.e., the intensities at which the earthquake was felt. According to descriptions reported by Zayakin and Luchinina (1987), significant destruction took place in Ust'-Kamchatsk, suggesting local intensities of 8–9 on the MSK scale, as opposed to, e.g., 6–7 in 1971. Distances from Ust'-Kamchatsk to the various proposed epicenters are shorter for solutions in the Kamchatskiy Peninsula (19 km to the ISC-GEM epicenter, 49 km to E.R. Engdahl's new solution, 43 and 45 km to the 1917 and 1971 epicenters, 50 km to the closest point of our Monte Carlo ellipse) than to the solutions inside the rupture area of the mainshock in the Gulf of Kamchatka (58 km to the ISS solution and 90 km to the Centennial Catalog's); however, these figures are not sufficiently different to allow ruling out any of the epicenters on this basis. Further use of this approach is hampered by the fact that macroseismic data is only available from one site—Ust'-Kamchatsk—and that the probable epicentral locations are located in an area which did not support any population in 1923 (and still does not for the most part).

In conclusion, in view of the results of modern relocations (ISC-GEM, this study, E.R. Engdahl), we regard as very improbable that the UK earthquake of 13 April 1923 was a genuine aftershock of Event M3 at the northern end of its rupture zone. It could have occurred at the same location as in 1917 and 1971, but with a moment estimated at half that of the 1917 event (see Sect. 3). It would be unlikely that an earthquake of that size would have followed the 1917 event at the same location, except in an aftershock context, which would then violate Utsu's (1970) law, predicting a difference of 1.1 magnitude units (as opposed to 0.2 in the present case) between a mainshock of the size of the 1917 earthquake and its maximum aftershock.

Rather, we propose that the UK event was displaced to the north, either inside the Kamchatskiy Peninsula, as suggested by the ISC-GEM, Engdahl, and for that matter, G–R solutions, or even at the Ozernoy Bight, in the southern part of our Monte Carlo ellipse.

We also note that Lake Nerpichye, which occupies a large fraction of the Kamchatskiy Peninsula to the north of Ust'-Kamchatsk, became salinized after the April 1923 event and remained brackish for several years (Gorin and Chebanova 2011). This suggests an invasion of seawater during the tsunami, with some resilience which could have been helped by coseismic deformation of the boundaries of the lake, as would be expected from an earthquake source located under the Kamchatskiy Peninsula, and possibly under the lake itself.

3. Estimates of Seismic Moment

In this section, we obtain seismic moments at mantle wave periods for the principal events of the 1923 sequence, as well as for the 1969 and 1945 Ozernoy Bight, and 1917 Cape Kamchatskiy earthquakes. Table 2 lists the available waveforms. For such historical events, and given the small number of records, it is impossible to invert a moment tensor, and we simply compute a mantle magnitude $M_c = \log_{10} M_0 - 20$ (M_0 in dyn cm), corrected for a probable focal mechanism (Okal and Talandier 1989). For earthquakes MS3 (mainshock), F2 and A12, we use a geometry representative of the subduction of the Pacific plate under Kamchatka ($\phi = 210°$, $\delta = 20°$, $\lambda = 90°$); for the other events, we also use the mechanisms published for the 1971 earthquake

Table 2

Seismic records used in moment estimates

Station	Code	Instrument	Distance (°)	Azimuth (°)	Phases used
Cape Kamchatskiy, 30 JAN 1917					
Göttingen, Germany	GTT	Wiechert	70.3	343	R_1
Main foreshock (F2), 02 FEB 1923					
Göttingen, Germany	GTT	Wiechert	72.6	342	R_1,G_1
Main shock (M3), 03 FEB 1923					
Cape Town, South Africa	CTO	Milne Shaw	146.4	292	G_1
De Bilt, The Netherlands	DBN	Golitsyn	71.7	344	G_1,G_2
Göttingen, Germany	GTT	Wiechert	71.4	341	G_1
La Paz, Bolivia	LPZ	Mainka	127.1	63	G_1
Strasbourg, France	STR	Wiechert	74.7	341	R_1
Uppsala, Sweden	UPP	Wiechert	62.1	340	R_1,G_1
Main aftershock (A12), 24 FEB 1923					
Göttingen, Germany	GTT	Wiechert	70.7	342	R_1,G_1
Tsunami Earthquake (UK13), 13 APR 1923					
De Bilt, The Netherlands	DBN	Golitsyn	69.0	346	R_1,G_1
Ozernoy Bight 22 NOV 1969					
L'Aquila, Italy	AQU	WWSSN LP	77.0	338	R_4,G_4
Mundaring, Western Australia	MUN	WWSSN LP	97.2	219	R_1,G_1,G_2
Tucson, Arizona	TUC	WWSSN LP	61.0	75	R_3
Windhoek, Namibia	WIN	WWSSN LP	137.3	311	R_3,G_3

($\phi = 276°$, $\delta = 21°$, $\lambda = 158°$; Okal and Talandier, 1986) and for the 1969 Ozernoy shock ($\phi = 225°$, $\delta = 16°$, $\lambda = 97°$, Cormier, 1975; and $\phi = 46°$, $\delta = 71°$, $\lambda = 38°$, Fedotov et al. 1973).

- For the mainshock (MS3; Fig. 3a–c), we were able to gather records on mechanical instruments at CTO, LPZ, UPP, STR and GTT, and on the Golitsyn electromagnetic seismograph at DBN (including a second passage G_2). This dataset suggests a moment of 5×10^{28} dyn cm at the longest available periods ($T > 170$ s); Fig. 3); this value is slightly larger than proposed by Kanamori (1977) on the basis of the aftershock area (3.7×10^{28} dyn cm), but in agreement with our earlier estimate (Okal 1992) based only on the UPP records (5.5×10^{28} dyn cm). Note also that it predicts a fault length of 225 km under Geller's (1976) scaling laws, in good agreement with the proposed distribution of aftershocks (260 km; Fig. 2).

- For the foreshock (F2, 02 FEB 1923, 05:07 GMT), the Love and Rayleigh wavetrains recorded at GTT are compatible with the low-angle thrust geometry and a moment of 2×10^{27} dyn cm, at mantle frequencies (5–6 mHz).

- In the case of the main aftershock (A12, 24 FEB 1923), the only records available (the GTT Wiecherts) suggest a slightly rotated subduction mechanism ($\phi = 225°$, $\delta = 20°$, $\lambda = 90°$) with a moment of only 8×10^{26} dyn cm.

- The lone record obtained for the 1917 earthquake (R_1 at GTT; the EW record holding the Love wave being too faint to process) cannot put constraints on its mechanism, but tentatively suggests a slow source, with a very strong increase of moment with period (slope of -0.22 logarithmic units per mHz on Fig. 3d), both in the strike-slip geometry of the 1971 earthquake, and in the less probable one of a low-angle subduction. The moment at mantle periods ($\sim 6 \times 10^{27}$ dyn cm) is equivalent to that
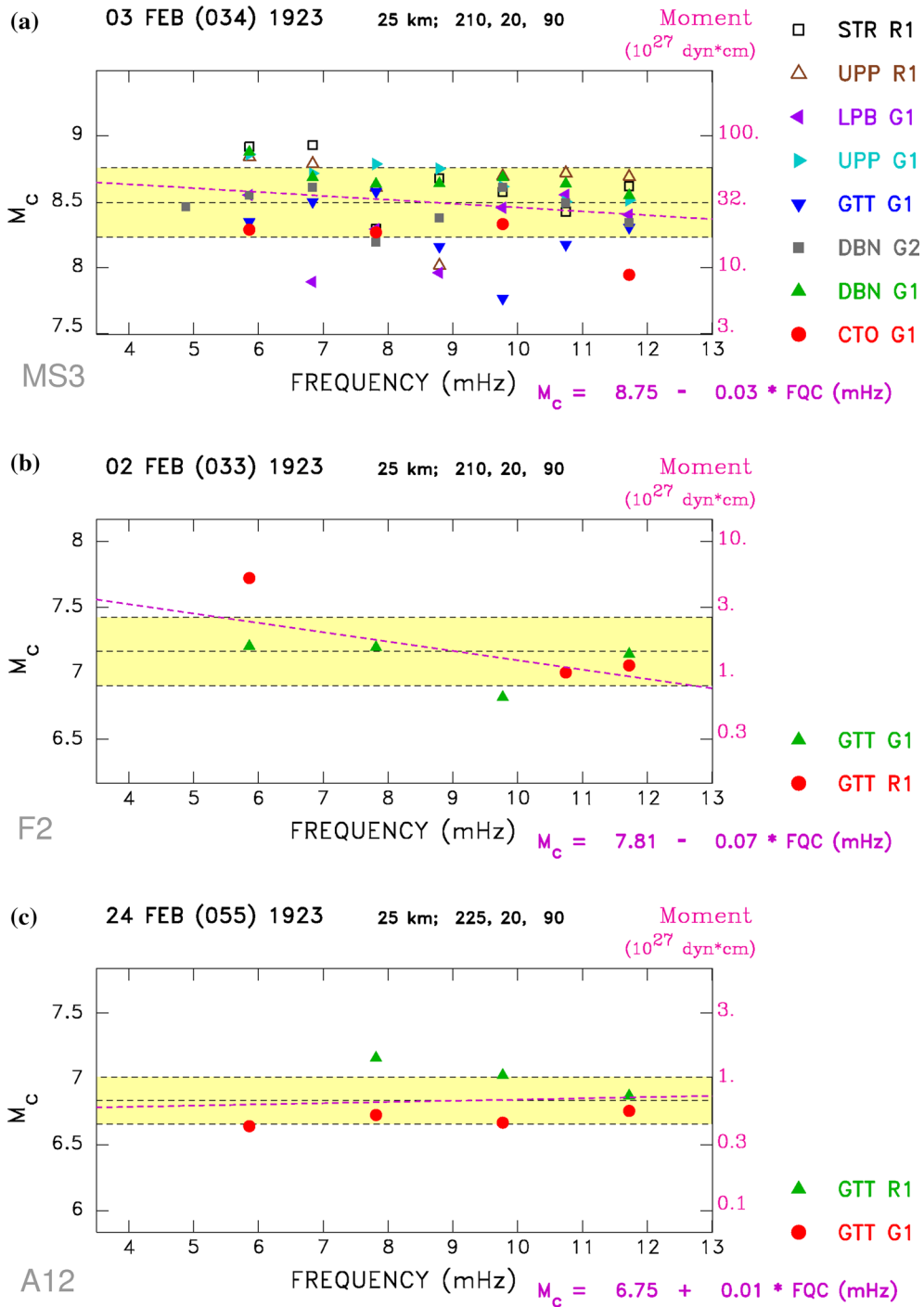
Figure 3
Mantle magnitudes corrected for focal mechanism, M_c (Okal and Talandier 1989) derived from spectral amplitudes of surface waves at mantle periods. The dashed lines and yellow band give the average and standard deviation of M_c over the entire frequency band, and the purple dashed line its linear regression. The depth and focal mechanism assumed in the correction are printed next to the date. **a** Mainshock (Event MS3); **b** Main Foreshock (Event F2); **c** Main Aftershock (Event A12); **d** 1917 Cape Kamchatskiy Event; **e** 1936 Cape Kamchatskiy Event
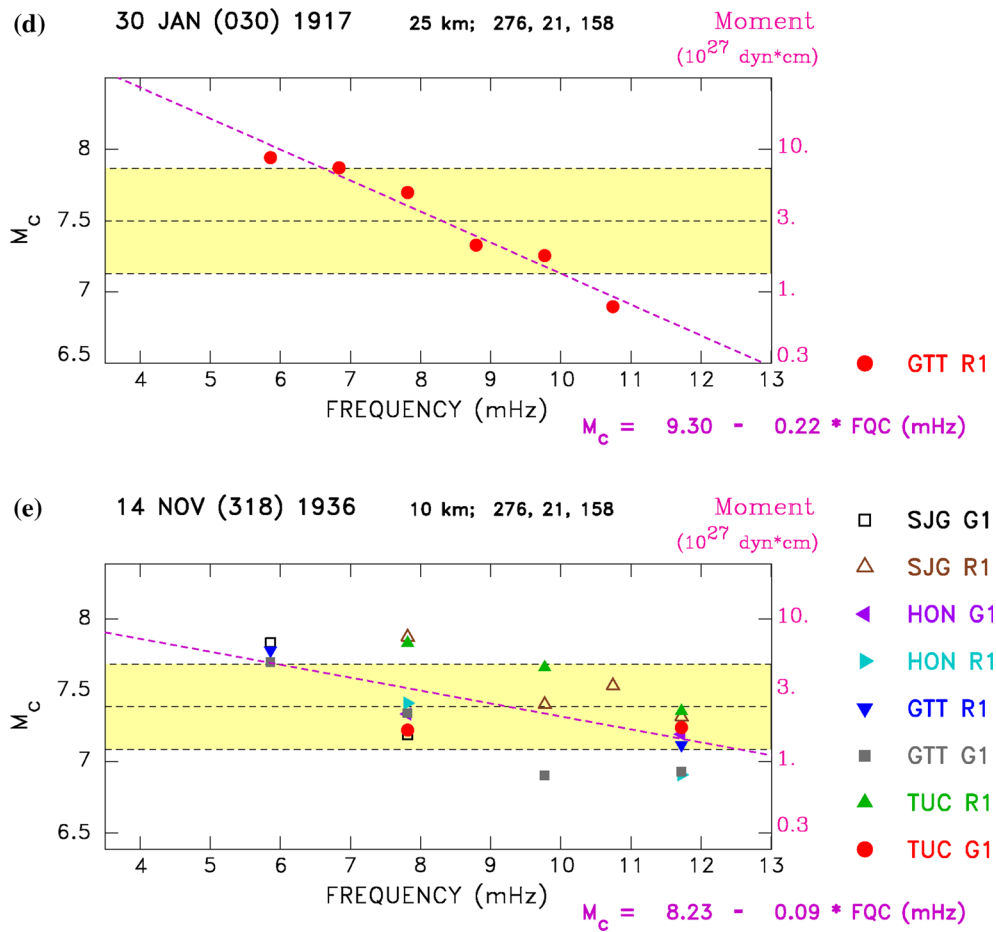
Figure 3
continued

in 1971, and the two earthquakes could then be repeats of each other, 55 years apart, with a seismic displacement of ~ 2.8 m, inferred from their common moment using Geller's (1976) scaling laws.

- In the case of the 1936 earthquake at Cape Kamchatskiy, the various spectral amplitudes are compatible with the oblique geometry of the 1971 event and a moment of about 4×10^{27} dyn cm (by contrast, a subduction geometry predicts a node of excitation of G_1 at HON which is not observed); that moment scales to 2.4 m of slip (Geller 1976) (Fig. 3e).

- In the case of the 1969 Ozernoy earthquake (Fig. 4), in addition to Fedotov et al.'s (1973) thrust mechanism, low angle thrust solutions were proposed by

Cormier (1975), Stauder and Mualchin (1976) and Daughton (1990). The latter used body-wave modeling to infer a complex source with a total moment of 5×10^{27} dyn cm, but did not consider a strike-slip solution, despite the lack of constraint on the slip angle. Using a representative selection of WWSSN records, we find that the low-angle thrust mechanism proposed by Cormier (1975) leads to an unacceptable scatter of moment values; in particular, it cannot reconcile the Love-to-Rayleigh ratios at Windhoek (WIN), as it would place the station in a node of excitation of Love waves. We prefer the mostly strike-slip mechanism of Fedotov et al. (1973), which predicts a more consistent set of moment values, reaching $\sim 3 \times 10^{27}$ dyn cm at mantle wave periods.
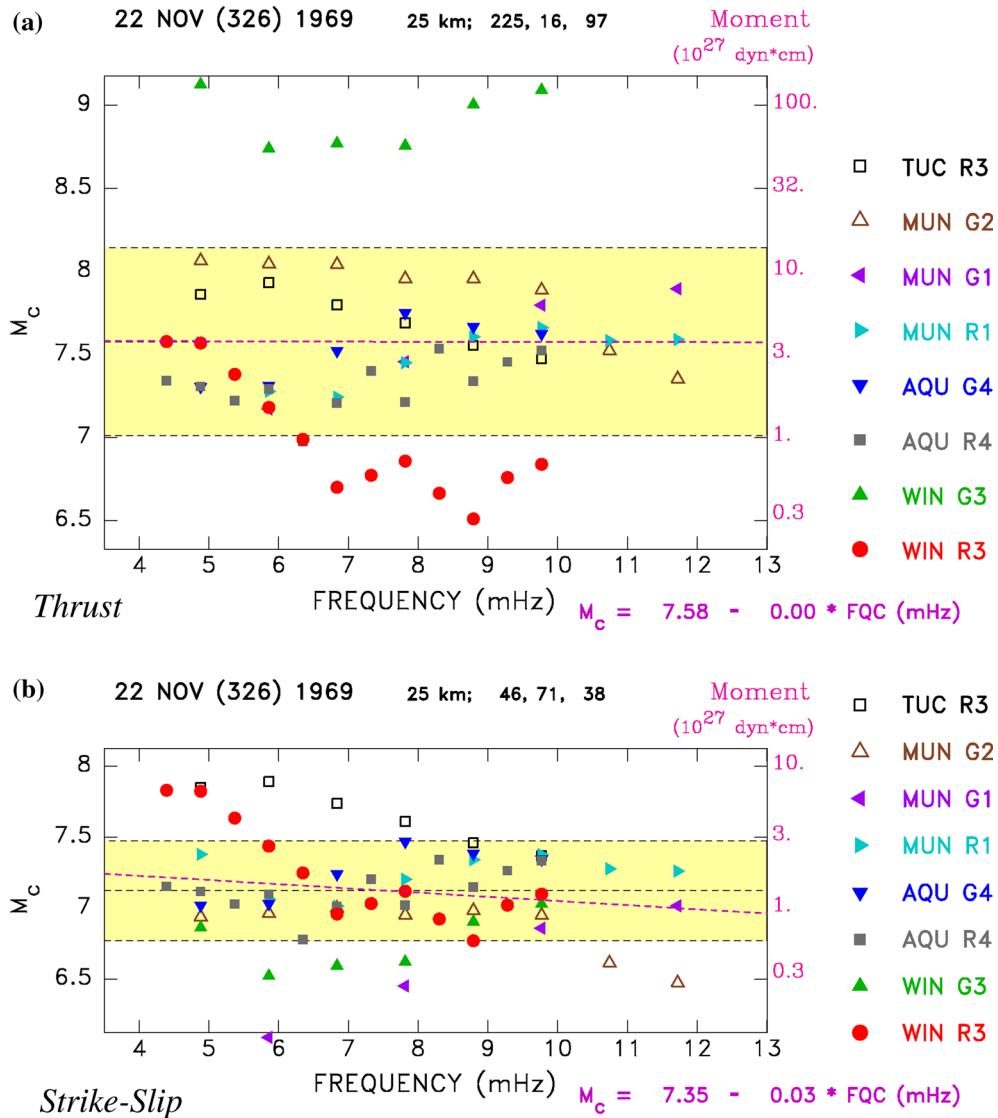
Figure 4

Same as Fig. 3 for the 1969 Ozernoy earthquake. **a** Thrust mechanism proposed by Cormier (1975); note the large scatter, notably for station WIN. **b** Preferred strike-slip mechanism (Fedotov et al. 1973); note improved fit to dataset

- By contrast, the 1945 earthquake, 90 km farther to the south, has spectral amplitudes better reconciled by Cormier's (1975) subduction geometry, than by Fedotov et al.'s strike-slip mechanism, with a suggested moment of 1×10^{27} dyn cm (Fig. 5). Note that no seismicity at a level comparable to the 1969 and 1945 events has occurred in the area since the start of the Global CMT catalog in 1976 (Dziewonski et al. 1981; Ekström et al. 2012).

- Finally, in the case of the UK tsunami earthquake of 13 April 1923, we could not obtain usable records at mantle periods from any Wiechert instruments (including at Göttingen), and could process only the two Golitsyn components at DBN. As shown on Fig. 6, the spectral amplitudes of Rayleigh and Love waves at DBN are best reconciled in the geometry of Fedotov et al.'s (1973) mechanism for the 1969 Ozernoy earthquake (with a moment of 1.0×10^{27} dyn cm
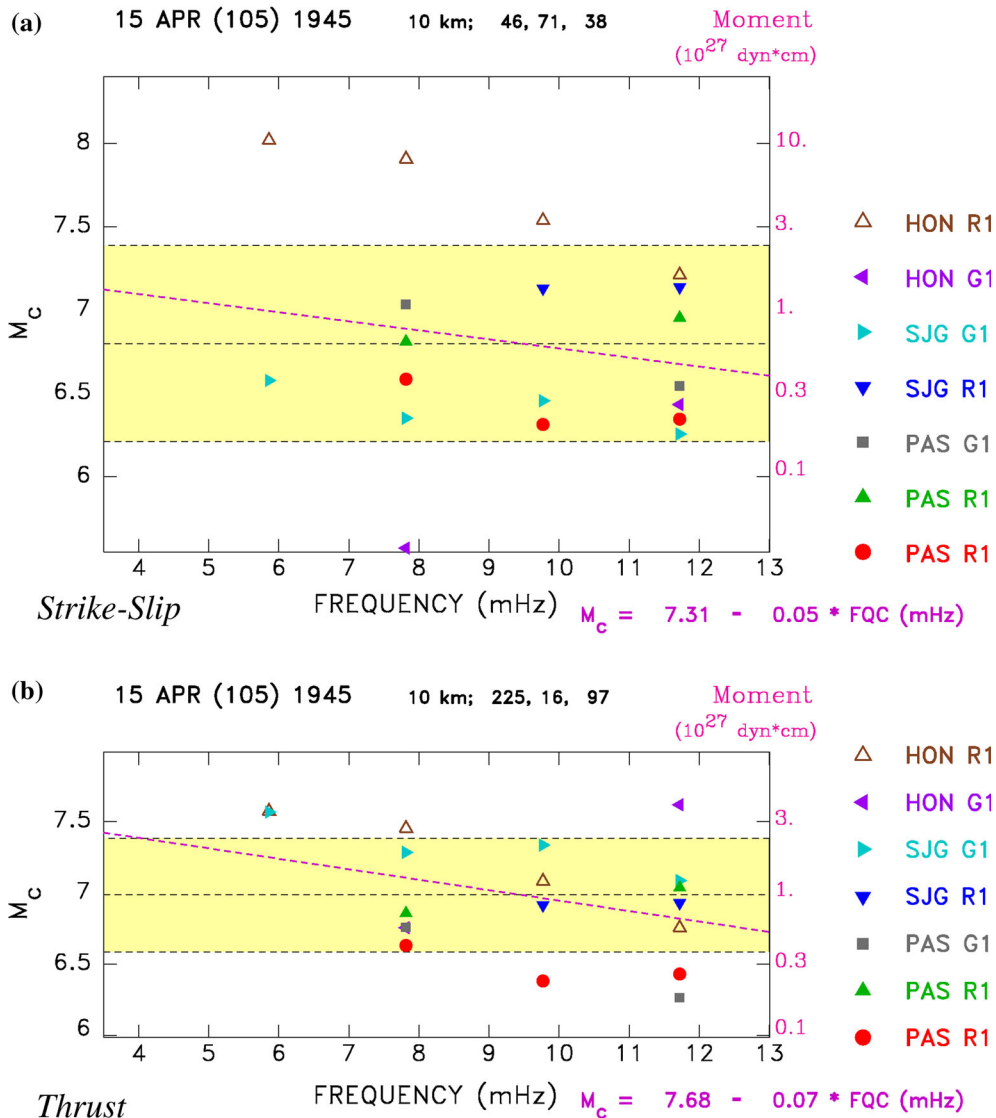
Figure 5
Same as Fig. 3 for the 1945 Ozernoy earthquake. Note that a strike-slip mechanism **a** gives a poor fit, notably to Rayleigh waves at HON. The thrust mechanism **b** is preferred

around 200 s), or of the 1971 oblique subduction (with a moment of 1.2×10^{27} dyn cm). Low-angle thrust subduction mechanisms predict much larger Love spectral amplitudes, which are not observed. This supports the model of the UK earthquake not being a genuine aftershock, but rather occurring by stress transfer outside the rupture area of the mainshock along the Kamchatka subduction zone. In the absence of adequate short-period

seismograms, it was not possible to quantify the slowness of the UK event through an Energy-to-Moment parameter Θ (Newman and Okal 1998), but a remarkable aspect of Fig. 6 is the growth of moment (or magnitude M_c) with period, the slope of the regression being -0.13 logarithmic units per mHz. This number is typical if not in excess (in absolute value), of those for other tsunami earthquakes, such as the 1932 Mexican, 2010 Mentawai
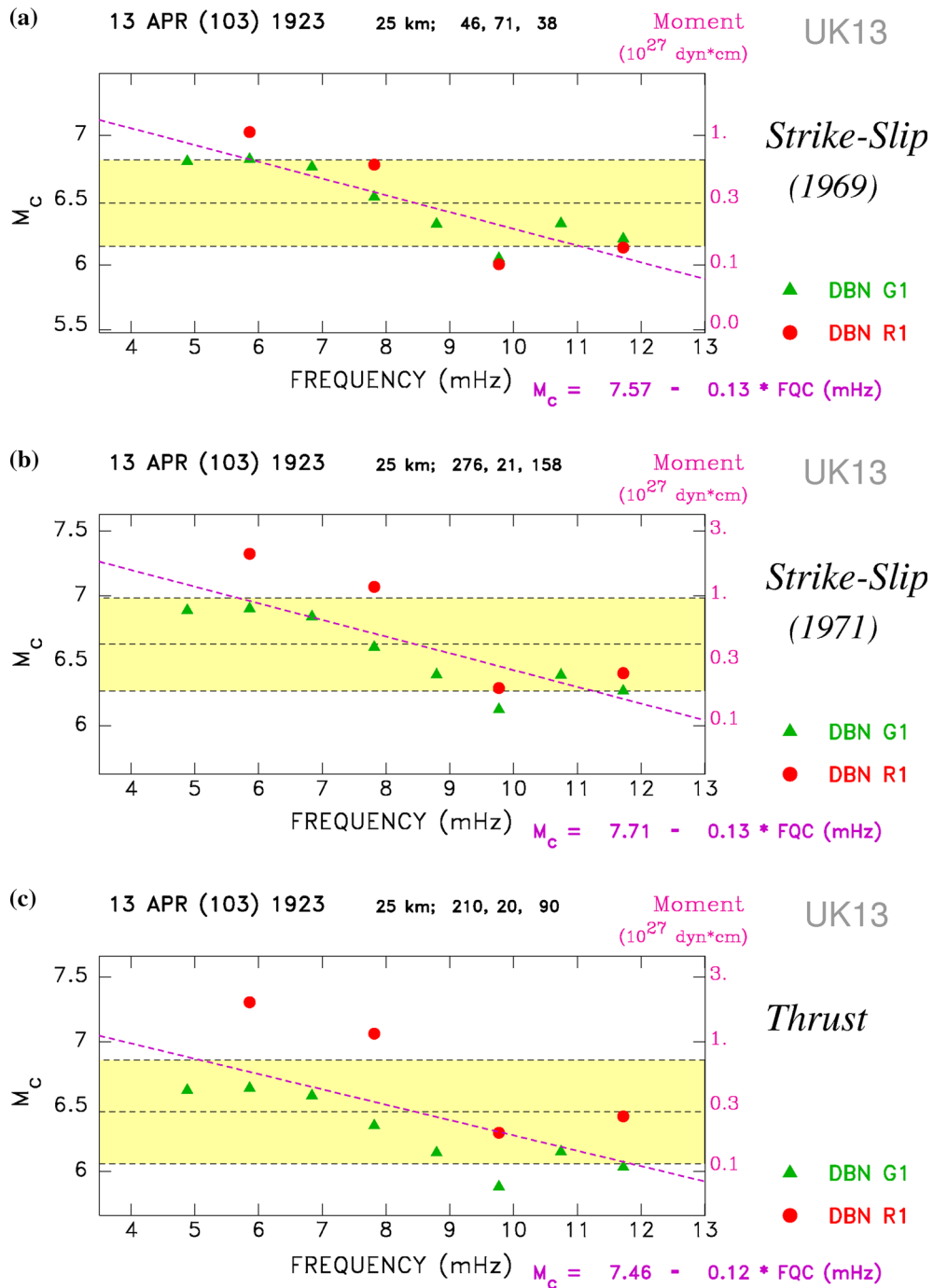
Figure 6

Same as Fig. 3 for the Ust'-Kamchatsk tsunami earthquake of 13 April 1923. Note that the spectral data fit the strike-slip geometries of the 1969 Ozernoy earthquake (**a**), and to a lesser extent of the 1971 Commander Islands event (**b**), better than the thrust fault one expected of a genuine aftershock (**c**). Note also the steep slope regressing M_c against frequency, which identifies the earthquake as slow
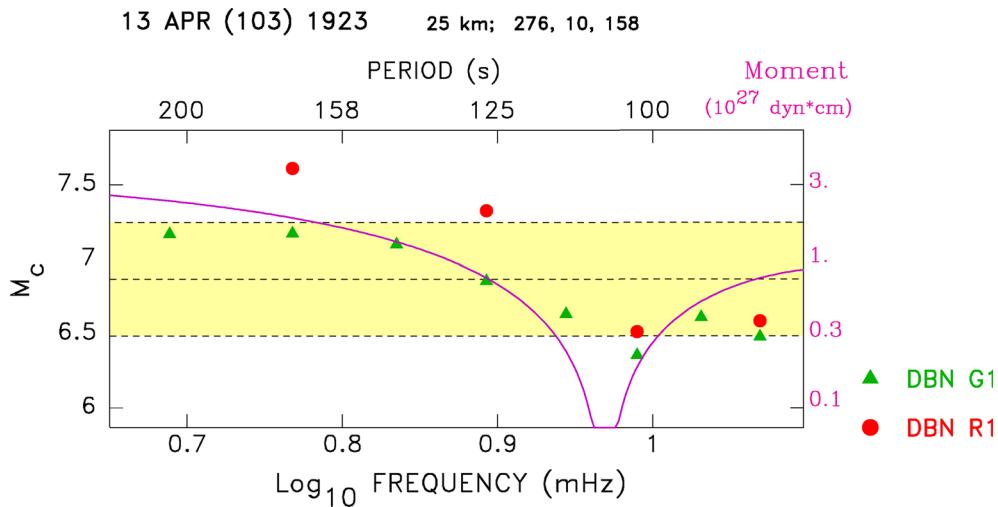
Figure 7

Same as Fig. 6b using a logarithmic scale for frequency. The solid purple line is a best fit of the spectrum of a classical sinc $\omega\tau/2$ moment release time function, suggesting a corner time $\tau \sim 100$ s

or both 1947 Hikurangi events (Okal and Borrero 2011; Okal 2011; Okal and Saloor 2017). This is in contrast to the mainshock (MS3) and the main aftershock (A12), for which the negative slopes on Fig. 3 are only -0.03 and 0.0 logarithmic units per mHz, respectively, suggesting that those events do not feature any anomalous source slowness. Note also that the UK event has both a larger moment and a smaller magnitude M_{PAS} than the main aftershock A12. In a more classical plot using a logarithmic scale for frequency (Fig. 7), we hint at a hole in the spectrum around 10 mHz, which is confirmed by a systematic grid search for static moment and rupture time, in the form of a classic sinc $\omega\tau/2$ moment release time function, yielding $M_0 = 3 \times 10^{27}$ dyn cm and $\tau \sim 100$ s, significantly longer than expected under classical scaling laws (Okal 2003), which could be explained by a slower rupture velocity. All these remarks confirm the slow character of the UK earthquake, and its nature as a tsunami earthquake. Incidentally, we note that Gusev (2004) has quantified the 1923 UK tsunami through a "tsunami magnitude" $M_t = 8.2$, which he then assigned to the parent earthquake, in the process noting that it was larger than its conventional seismic magnitude, $M_s^{(GR)} = 7.2$. This procedure is questionable since it tacitly assumes that the tsunami was fully generated by the

earthquake; it becomes very unfortunate when, in subsequent publications, this value is then equated to a moment magnitude M_w, leading for example Bourgeois and Pinegina (2017) to describe the MS and UK events as a kind of pair, when their seismological properties clearly advocate a large difference in size. In short, the UK event cannot have a moment for its dislocation as high as 2.5×10^{28} dyn cm, ($M_w = 8.2$), as used for example by Bourgeois and Pinegina (2017), since this would lead to vertical ground motion spectral amplitudes of 5 mHz Rayleigh waves at Göttingen ($\Delta = 70°$) on the order of 20 cm.s, corresponding in turn to time-domain zero-to-peak amplitudes of ~ 2 mm, or an easily detectable 1.5 cm on a horizontal mechanical instrument with a magnification of ~ 10 in that frequency band (Okal and Talandier 1989).

4. Tsunami Investigations

Before proceeding to simulations of the tsunami of 13 April 1923, we review tsunami data documented in the vicinity of Cape Kamchatskiy, either from actual observations during the 1923 and other
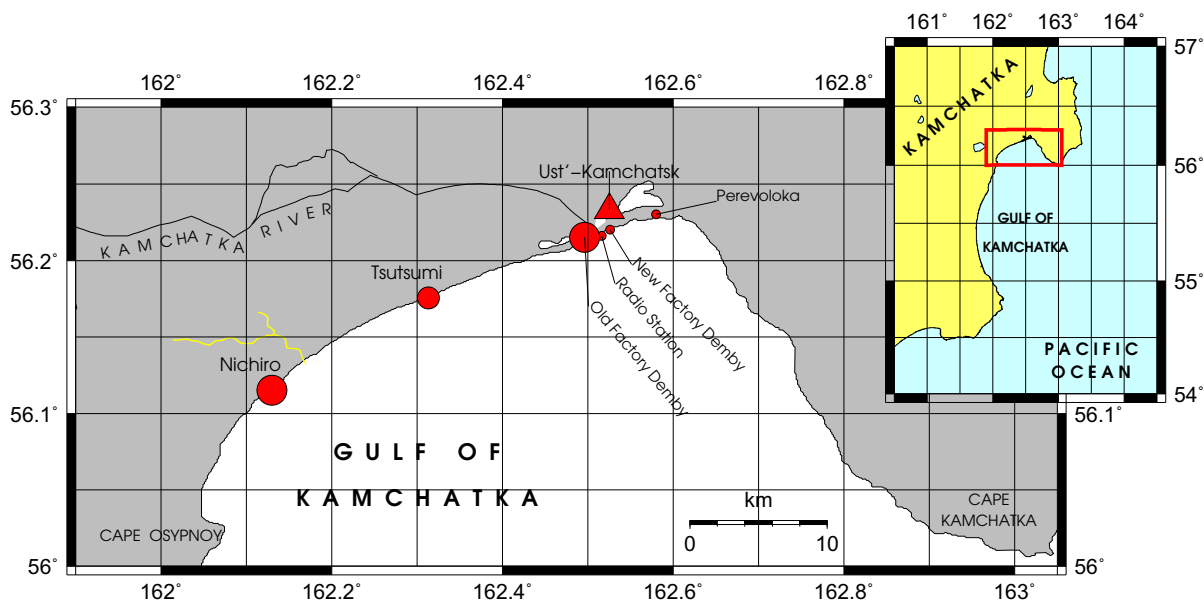
Figure 8
Area affected by the 13 April 2013 tsunami, as reported by Troshin and Diagilev (1926) and Soloviev and Ferchev (1961). The highest reported run-ups were documented on the Demby landspit (11 m) and at Nichiro (20–30 m). The yellow line is our best interpretation of Soloviev and Ferchev's First Creek

events at the very few past or present settlements along the coast, or from sedimentological work by Bourgeois et al. (2006), Martin et al. (2008) and Bourgeois and Pinegina (2017), for which age estimates can be bracketed by ash deposits from known major eruptions at the nearby volcanoes Bezymianniy and Shiveluch.

- *13 April 1923* Detailed reports of the tsunami following the UK event by Troshin and Diagilev (1926) have documented large run-up values reaching 20–30 m, with the tsunami affecting the northern coastlines of the Kamchatskiy Bight, from Cape Shubert to Cape Kamchatskiy (Fig. 8). According to Soloviev and Ferchev (1961), a first and small wave arrived at Ust'-Kamchatsk 15 min after the earthquake, "at approximately 02:15",[1] followed 15 min later by a second catastrophic wave rising up to 11 m, destroying the structures at

Demby, and flowing 7 km into the mouth of the Kamchatka River; note however that Minoura et al. (1996) have argued that this exceptional penetration was facilitated by the gliding of the waves over a coastal plain covered by a thick layer of frozen snow. Higher run-up values occurred to the west of the Kamchatka River, with the maximum value of 20 m (Soloviev and Ferchev 1961) or 20–30 m (Zayakin and Luchinina 1987 reported at Nichiro, where the canneries were totally destroyed, as well as at Tsutsumi. In this context, Borisov (2002) reports (presumably based on Troshin and Diagilev (1926)) that a small cutter from the Nichiro cannery was deposited on a 30-m terrace at the location Gorbusha, which we interpret to lie 1–2 km inland, at the back of a coastal plain gently rising to an altitude of no more than 6 m. As such, the documented heights of 20–30 m do represent run-up on a sloping beach, as opposed to a splash on a steep cliff. By contrast, and according to Soloviev and Ferchev (1961), themselves quoting from Troshin and Diagilev (1926), the waves (and consequent damage) decreased eastward, notably over a distance of ∼ 10 km along the spit

---

[1] Note here an inconsistency in absolute timing since the origin time of the event is 15:31 GMT, or 02:31 local time on the 14th. The legal time in Kamchatka was GMT+11 in 1923; it was advanced one hour in all time zones of the USSR in 1930, and hence would have been GMT+12 in 1971 (see below).

separating Lake Nerpichye from the ocean. There, the old Demby cannery at the western end was destroyed, the radio station and the new cannery at its center were only partially affected, and the water rose a mere ~ 1 m at Perevoloka, at its eastern end (Zayakin and Luchinina 1987), although this interpretation has been questioned in the context of the salinization of Lake Nerpichye in the 1920s (Gorin and Chebanova 2011). Finally, and according to Soloviev and Ferchev (1961), the tsunami reached a maximum run-up of 4 m at Nikol'skoye (Bering Island), although the exact location of this report and hence the relevant morphology of the coastline is unknown. The tsunami also produced a 30-cm wave at Hilo, Hawaii; 20 cm at Honolulu, Hawaii; 8 cm at Tofino, B.C.; 15 cm at San Francisco; and swirls in Los Angeles harbor. The latter are described as taking place between 6 and 10 a.m. on the 14th (The Los Angeles Times 1923), i.e. between 14:00 and 18:00 GMT. This can be interpreted as a delayed harbor resonance upon arrival of waves propagating outside the shallow-water approximation, as observed at distant harbors during the 2004 Sumatra tsunami Okal et al. (2006a, b). The timing would be reconciled with 100-s waves propagating at a group speed of 87 m/s in an ocean averaging 4.5 km in depth, over a distance of 7000 km (detouring around the Aleutian island chain), but the non-linear nature of the resonance precludes any quantitative interpretation. The same article (The Los Angeles Times 1923) mentions a devastating inundation of the Korean coast north of Pusan, with more than 1000 lives lost, but that disaster apparently occurred at least 24 h prior to the UK earthquake, and is, therefore, unrelated. In seeking to simulate the tsunami of 13 April 1923, the critical dataset to be modeled will consist of the local tsunami amplitudes of 11 m at Demby and more than 20 m at Nichiro, of the much weaker ones at Perevoloka, and to a lesser extent of the decimetric amplitudes in Hawaii and along the Pacific coast of North America.

- *15 December 1971* The tsunami was registered with an amplitude of 47 cm at Ust'-Kamchatsk, but was apparently not observed visually, due in part to its occurrence at low tide (Soloviev et al. 1986).

Martin et al. (2008) later attributed to the 1971 event deposits identified at heights of 10 m on the Kamchatskiy Peninsula (56.19°N; 163.35°E). It is unclear how such a run-up could have remained undetected by the ~ 10 people manning the lighthouse and weather station at Cape Afrika (altitude 7–8 m), even taking into account the night-time occurrence of the event (solar time $\sim 19{:}23$; legal time 20:30 GMT+12). On the other hand, and despite the seismic similarity between the events of 1917 and 1971, comparable tsunami effects in 1917 might have gone unnoticed if that location had been uninhabited, a reasonable assumption given that the lighthouse was built in 1960. In this context, it is worth noting that Bourgeois et al. (2006) describe tsunami deposits at Stolbovaya Bay (56.68°N; 162.92°E), intertwined between the tephra layers of 1854 (Shiveluch) and 1956 (Bezymianniy), for which they discount the 1923 event as a possible origin (and suggest that the deposit may result from the 1945 event), based on a comparison of the relevant run-up (5–6 m) with that reported in 1923 for Bering Island (4 m). This argument tacitly assumes a 1923 epicenter in the Pacific Ocean south of Ust'-Kamchatsk for which the distance to Stolbovaya would be greater than to Bering Island; if, as we have argued, the UK epicenter is either in the Kamchatskiy Peninsula, or north of it, the argument fails, and the deposits in question may have come from the 1923 UK event, which is also larger than the 1945 source.

- *22 November 1969* A very significant tsunami was reported north of the Kamchatskiy Peninsula, principally along the Ozernoy Bight, where run-up was described as having reached 12–15 m at a then existing meteorological station at the mouth of a river Ol'khovaya (literally, river of the alders) (Fedotov et al. 1973); the interpretation of this report is made difficult by the existence of two rivers by that name, with mouths at 57.12°N, 162.80°E and 57.62°N, 163.23°E, respectively (Anonymous 2001); the authors' Fig. 6 would support the latter location. The tsunami was also reported as far north as Lavrov Bay (60.3°N; 167.2°E), 400 km from the epicenter (Fedotov et al. 1973). By contrast, it was recorded with a

minimal amplitude (27 cm) at Ust'-Kamchatsk. Martin et al. (2008) conducted a sedimentological investigation of tsunami deposits along Ozernoy Bight, confirming run-ups on the order of 5–7 m, but casting doubt on the larger value reported by Fedotov et al. (1973) at Ust' Ol'khovaya; however, neither of the two possible locations was sampled by the authors.

- *30 January 1917* No tsunami reports are available for this earthquake, despite a daylight occurrence (origin time 02:45 GMT or 13:37 solar time), and its similarity with the 1971 event. We note however that seven out of the ten Pacific-wide maregraphs having reported the 1971 tsunami do not appear in the NOAA run-up database until 1933, with two more reporting only amplitudes larger than 10 cm until 1927, which may explain the lack of observations.

4.1. Hydrodynamic Simulations

We simulate the Kamchatka tsunami of 13 April 1923, using the MOST algorithm (Titov and Synolakis 1995; Titov and González 1997; Titov and Synolakis 1998) which solves the non-linear shallow water approximation of the Navier-Stokes equations. It has been extensively validated against actual tsunami surveys and laboratory experiments (e.g. Synolakis et al. 2008; Titov et al. 2016).

The bathymetry grid used in our simulations was digitized from Russian marine maps (Anonymous 2001), considerably more precise than available global models such as GEBCO (Fisher et al. 1982), especially in the immediate vicinity of Ust'-Kamchatsk (Fig. 9). We use several interpolations of the grid, the finest one at a resolution of 7.5 arc-seconds for smaller scale sources. The simulation time series were recorded at 41 virtual gauges located near the shoreline of the Gulf of Kamchatka.

4.1.1 Modeling an Earthquake Source

Following standard practice, we calculated static displacements from the earthquake source, to be used as initial values of the hydrodynamic simulations, using Mansinha and Smylie's (1971) algorithm. In the absence of a fully constrained focal solution for the UK event, we assumed the focal mechanism proposed by Fedotov et al. (1973) for the 22 November 1969 event, and approximated the fault dimensions from the event's size using earthquake scaling laws (Geller 1976). Because we could only use records from one station in our calculation of the seismic moment from mantle waves ($M_0 = 3 \times 10^{27}$ dyn cm), we used three magnitudes of $M_w = 7.0$, $M_w = 7.6$, and $M_w = 8.0$, with the second magnitude as our preferred result (Fig. 7), and the former and the latter as lower and higher end members.
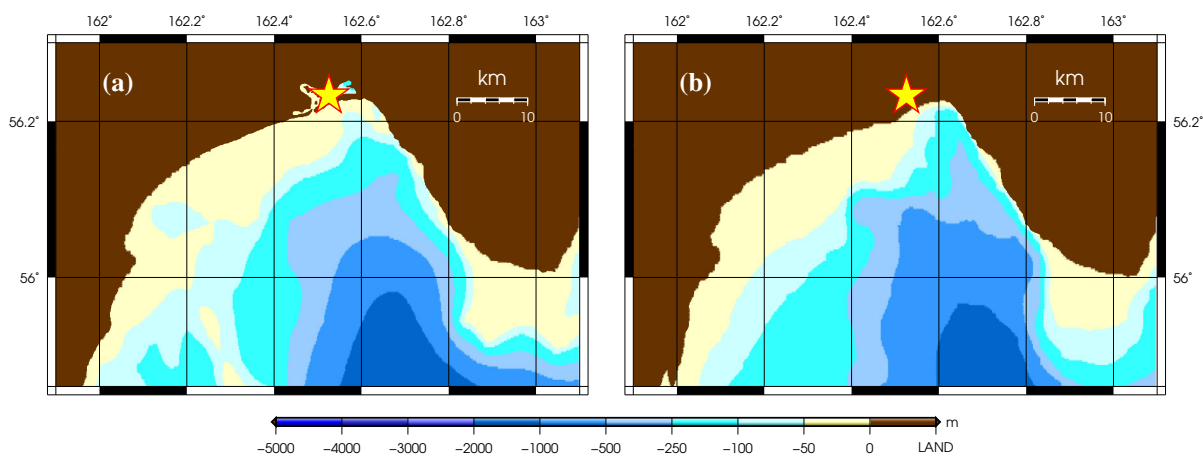

Figure 9
Bathymetry of the Gulf of Kamchatka **a** from the GEBCO global model (Fisher et al. 1982) and **b** digitized from a Russian marine map of Kamchatka (Anonymous 2001). The yellow stars in both figures depict Ust'-Kamchatsk
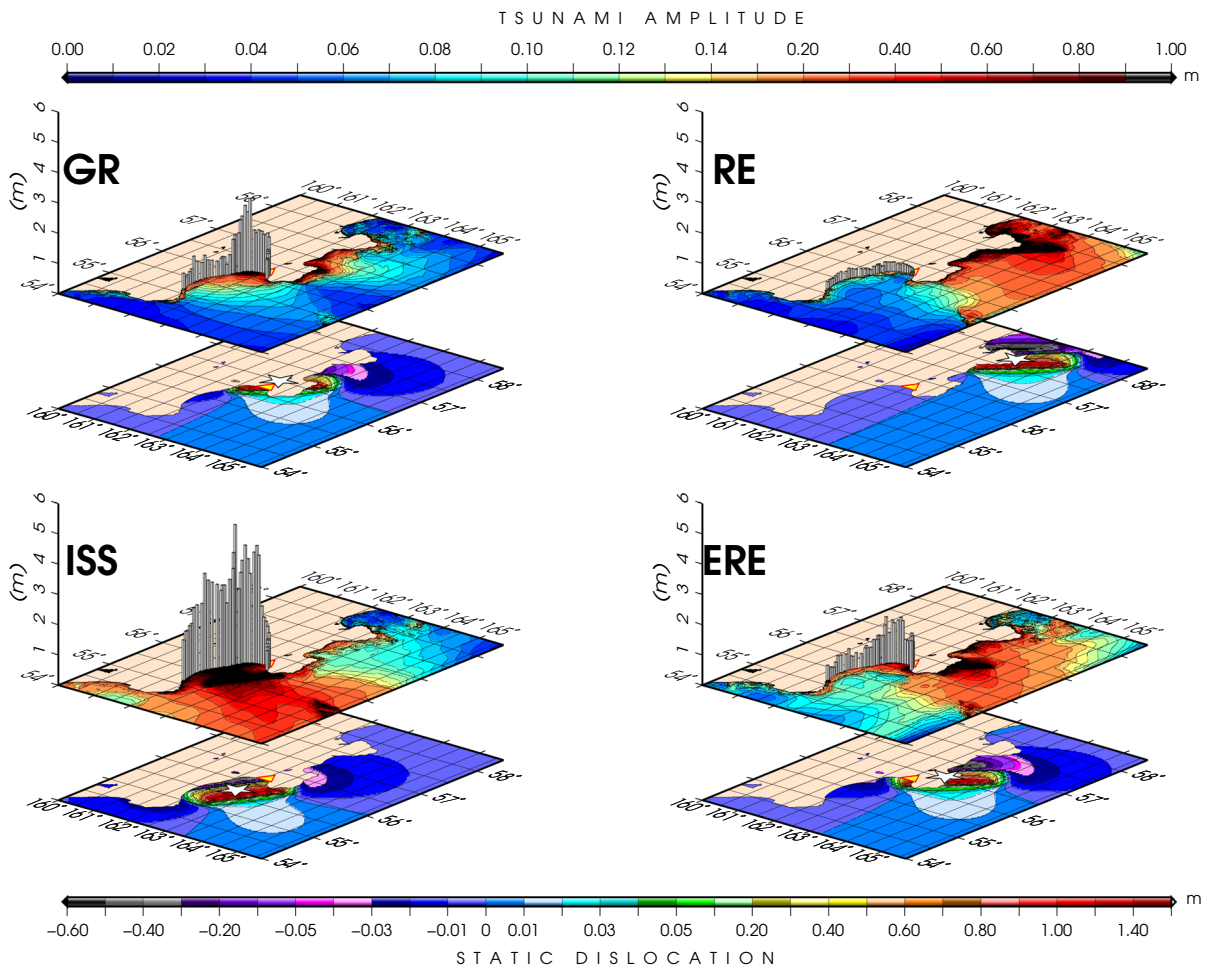
Figure 10
Static displacement maps (bottom slices) as well as simulation results (top slices) for the maximum magnitude ($M_w = 8.0$) considered in this study. Results for each scenario are labeled accordingly. Triangles and stars in all figures represent Ust'-Kamchatsk and the corresponding epicenter in each scenario. The gray vertical columns show the maxima of calculated amplitudes at the 41 gauges along the coastline of Gulf of Kamchatka

As to the event's location, we tested four different scenarios as discussed in Sect. 2. We label the location scenarios as GR (Gutenberg–Richter), ISS, ERE (Engdahl relocation)) and RE (the relocated epicenter in this study) as shown in Figs. 1 and 10. In the case of the ISS location, we use the thrusting mechanism in Fig. 6c.

We used time steps of $\Delta t = 1$ s during 12-hr windows in a grid with a resolution of 23 arc-seconds to satisfy the CFL conditions (Courant et al. 1928). This resolution is valid for the coarse grid as prescribed e.g. by Shuto et al. (1986) and Titov and

Synolakis (1995, 1997). We ended the calculations at a depth of 4 m near the coastlines and, therefore, assumed the calculated amplitudes at the virtual gauges along the coastline as proportional but not equal to the actual documented run-ups.

Figure 10 shows the static displacements (bottom slices) as well as fields of maximum calculated amplitudes (top slices) for a maximum assumed magnitude of $M_w = 8.0$, for all four possible locations.

Simulations from our relocated epicenter (RE) or the customized Engdahl relocation (ERE) produce
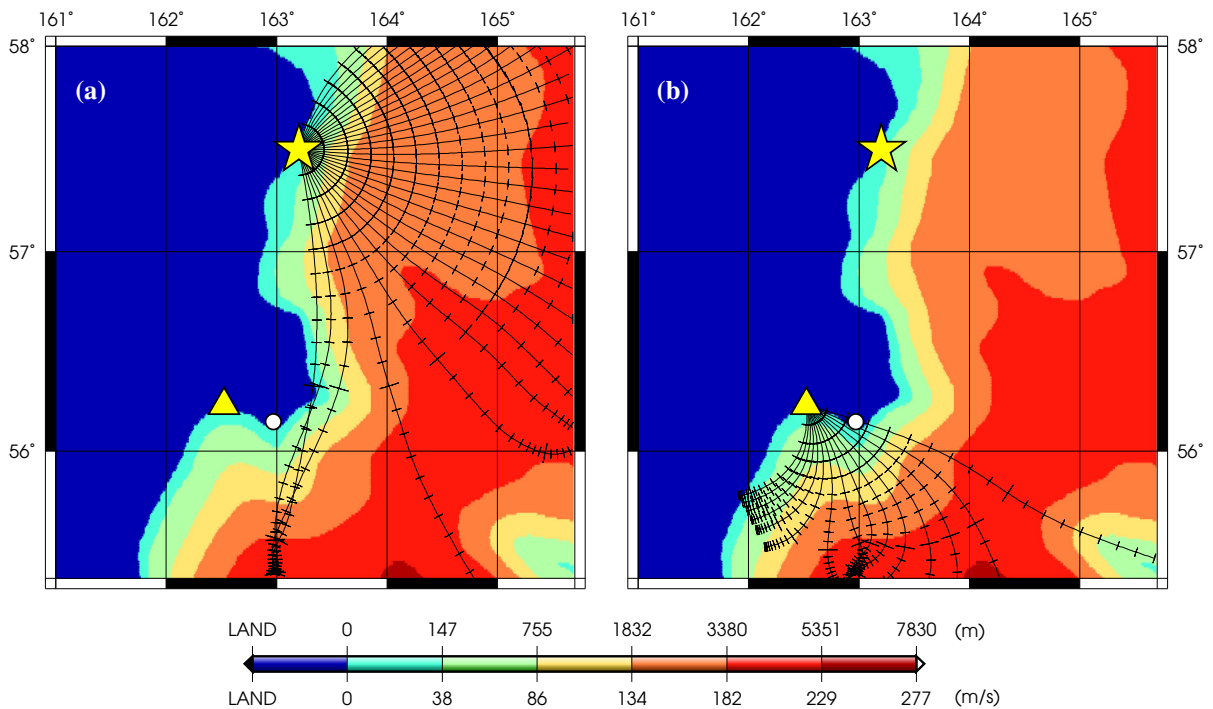
Figure 11
Tsunami ray tracing experiment from our relocated epicenter. Black curves represent tsunami rays, with the tick marks at every minute. The background undispersed velocity field is calculated from our bathymetry grid. The scale is measured for both depth (top) and velocity (bottom). In (**a**) the source is set at the relocated epicenter (RE, star), while (**b**) is a reverse diagram centered on the receiver at Ust'-Kamchatsk (triangle). The white dots represent Cape Kamchatskiy

only minimal amplitudes in the Gulf of Kamchatka (maximum ~ 1.5 m), making it improbable to reach the observed run-up amplitudes; the ISS source would generate higher amplitudes, but their distribution along the coast remains broad, illustrating the dimensions of the source (Okal and Synolakis 2004). The GR scenario (top left on Fig. 10) gives a better distribution of amplitudes along the coast, but they remain too weak (maximum ~ 2.4 m) to justify an observed run-up of 20 m on a very flat beach. Thus, none of the four possible scenarios yields satisfactory fields of amplitudes along the Kamchatskiy Bight.

4.1.1.1 Ray-Tracing Experiments   The inability of a northern source, such as RE or ERE, to efficiently inundate the coasts of the Kamchatskiy Bight can be further examined by ray-tracing experiments, following the techniques of Woods and Okal (1987) and Satake (1988). We apply Jobert and Jobert's (1983) solution of the 2-D Eikonal equations on a

heterogeneous sphere using a field of variable propagation velocities in the shallow-water approximation, to trace tsunami rays from our relocated epicenter using a 4th-order Runge-Kutta scheme. While some energy would be expected to diffract around the Kamchatskiy Peninsula in violation of geometrical optics (assumed by the ray-tracing methodology), this experiment provides a general illustration of the expected distribution of wave energy in the region.

As shown in Fig. 11a, a tsunami originating at our relocated epicenter (RE; yellow star) does not reach Ust'-Kamchatsk (yellow triangle), the rays approaching the Kamchatskiy Peninsula being focused by the shallow bathymetry into the deeper parts of the Kamchatskiy Bight, its northern coast thus being masked from the source by the Peninsula. In addition, using the concept of seismic reciprocity (Aki and Richards 2002), we can predict that no high amplitudes would be observed in Ust'-Kamchatsk from any

source located north of Cape Kamchatskiy (Fig. 11b). Note that this result is independent of the nature of the tsunami source, and would equally apply to a landslide source, as studied below.

4.1.2 Landslide Sources

Having ruled out any of the legitimate earthquake scenarios as the source of the 13 April 1923 tsunami, we next consider the possibility of a landslide source. Generation of major tsunamis by underwater landslides triggered by large earthquakes has been documented in numerous instances, including the catastrophic events of 1998 in Papua New Guinea (Synolakis et al. 2002) and 1946 in the Aleutians (Kanamori 1985; Fryer and Watts 2001; Okal et al. 2003; von Huene et al. 2014). Even earthquakes with epicenters located significantly onland have created tsunamigenic offshore landslides, with recent examples documented in 1954 and 1980 at Orléansville/El Asnam (Soloviev et al. 1992), 1990 on the southwestern slopes of the Caspian Sea (Salaree and Okal 2015), and 2013 in Pakistan (Hoffmann et al. 2014), the record triggering distance (900 km) being for the 1910 Rukwa earthquake (Ambraseys 1991).

Modeling landslides as potential sources for this event is motivated by the local nature of the tsunami, whose maximum amplitudes are concentrated along a short (~ 35 km) stretch of relatively straight coastline between Cape Osypnoy and Ust'-Kamchatsk (Fig. 8), beyond which the amplitudes fall sharply reaching only 1 m at Perevoloka (Soloviev and Ferchev 1961). While the dataset of reported run-ups is insufficient to compute a formal aspect ratio of its distribution, this observation fits qualitatively Okal and Synolakis' (2004) model.

The triggering of an underwater landslide by an earthquake requires two conditions: an adequate slope to carry the slide and a sufficient acceleration to destabilize its material. Regarding the former, we have obtained numerically the gradient of the bathymetric grid used in our simulations and present in Fig. 12 its modulus and azimuth (direction of steepest descent), following the technique used in previous studies (Okal et al. 2014; Salaree and Okal 2015). Underwater slumps have generally been observed on slopes between $\sim 3\%$ and $\sim 6\%$, the upper bound

reflecting the capacity of the slope to hold the precarious material; they can also take place on slopes as low as $\sim 1\%$ in very shallow waters (e.g. Skempton, 1953; Prior et al. 1982; Brunsden and Prior, 1984). Figure 12 shows that such slopes are amply documented in the Kamchatskiy Bight. In addition, we note an abundance of aerial slides along the eastern shore of the Kamchatskiy Bight, between Ust'-Kamchatsk and Cape Kamchatskiy (Fig. 13), suggesting the possibility of such mass failures on the sea floor, under the assumption of a morphological continuity between onland and offshore slopes, as suggested by Kawata et al. (1999) in the case of the 1998 Papua New Guinea event.

As for the peak accelerations expected from the UK earthquake at the proposed slide locations, they will obviously depend on the epicenter, focal geometry and source spectrum of the event, neither of which is fully constrained. Simulation of peak ground acceleration, using the algorithm by Campbell and Bozorgnia (2003), for the RE and ERE epicenters, predicts maximum vertical accelerations of, respectively, $0.03 \pm 0.01 g$ and $0.09 \pm 0.03 g$ in the northern Gulf of Kamchatka (Fig. 14) for $M_w = 7.6$. Although the former does not seem sufficient to trigger a landslide, the latter is about the triggering threshold (0.1 g) as proposed by Keefer (1984). Possibly larger seismic moments such as $M_0 = 1.0 \times 10^{28}$ or $M_w \approx 8$ may increase these values, although the slow nature of the source may limit their efficiency at the high frequencies controlling ground acceleration. Notwithstanding this reservation and irrespective of its exact source parameters, we note that the earthquake was felt at MMI VI in Ust'-Kamchatsk (Soloviev and Ferchev 1961), corresponding to peak accelerations of 0.1 to 0.2 g (Wald et al. 1999) which provide ample justification to the hypothesis of an underwater landslide in the Kamchatskiy Bight, only 30 km away, a location with ample sediment discharge by the Kamchatka River draining the volcanic province of Central Kamchatka (Kuksina and Chalov 2012).

In order to simulate the landslide tsunami, we used the block model approach for landslides as proposed by Synolakis et al. (2002). Following Salaree and Okal (2015) we model the slide as an instantaneous hydrodynamic dipole consisting of a trough and a hump of respective (positive) amplitudes
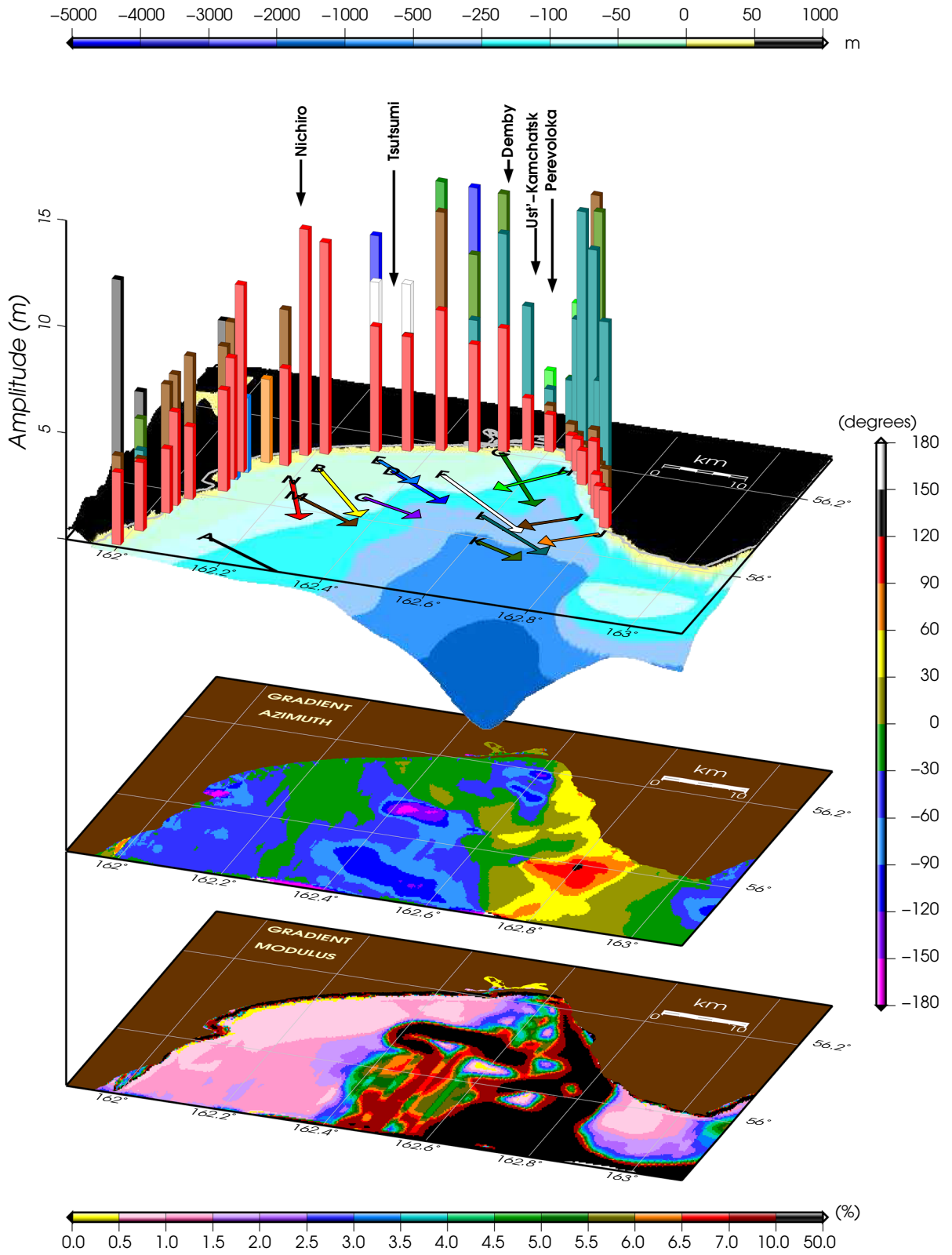
◄Figure 12
(Bottom) Modulus of the gradient field calculated from bathymetry; (middle) azimuth of the bathymetry gradient field; (top) 3-D bathymetry of the northern Gulf of Kamchatka with arrows representing the designed landslide dipoles in tsunami simulations. Maximum simulated amplitudes from the landslide scenarios at each of the 41 gauges are shown as vertical columns which are color-coded to match their corresponding arrows

η_- and η_+, separated by a lever of length l in the direction x of steepest descent, with a Gaussian profile along x and a sech^2 one across it, the initial deformation thus taking the form (Okal et al. 2009)

$$\eta(x, y; t = 0_+) = -\eta_- \exp(-\alpha_- x^2) \cdot \text{sech}^2(\gamma_- y)$$
$$+ \eta_+ \exp(-\alpha_+(x - l)^2) \cdot \text{sech}^2(\gamma_+ y) \quad (1)$$

We applied time steps of $\Delta t = 0.4$ s over 12 h time spans in our digitized grid interpolated down to 7.5 arc-seconds in order to accommodate a sufficient number of grid points per wavelength (e.g. Shuto et al. 1986). We designed 14 landslide scenarios (Table 3) following the slope map of the Gulf of Kamchatka calculated from our bathymetry grid as shown on the two bottom slices in Fig. 12. The columns in the upper slice in Fig. 12 indicate the maximum calculated amplitudes at 25 virtual gauges along northern margins of the Kamchatskiy Bight.

These columns are color coded to match their corresponding slide scenario in the Bight. As readily seen in Fig. 15 and detailed below, only slide scenario (N) provides an acceptable wave amplitude offshore of Nichiro, and an appropriate fall-off farther northeast along the shore.

In order to analyze the stability of the model (N) solution, we varied the dipole length from 5 to 15 km and its azimuth from 150° to 160°, in unit increments and recorded the time series at Nichiro. We then selected maximum amplitudes at 25 gauges (Fig. 15). The result, in Fig. 16, shows that the suggested dipole is stable, in the sense that the highest amplitudes are concentrated around Nichiro with amplitudes falling to 1–2 m at Perevoloka, as best demonstrated with the average of all the curves (red curve in Fig. 16).

In conclusion of this section, Model (N), featuring an underwater slide initiating at 56.065°N, 162.200°E and sliding 10 km along a local slope of 1–2%, in the azimuth 155°, with a total volume of 0.4 km^3, gives a satisfactory model to the fundamental observations available for the tsunami of 13 April 1923, namely the peak run-up of ~ 20 m at Nichiro and its rapid northeastward decay, reaching only 1–2 m at Perevoloka. It could easily have been triggered by

Table 3

Dipole model parameters

Model	Head (trough)					Lever		Hump		
	Lat. (°N)	Lon. (°N)	η_- (m)	α_- (km^{-2})	γ_- (km^{-1})	l (km)	Az (°)	η_+ (m)	α_+ (km^{-2})	γ_+ (km^{-1})
A	55.90	162.14	25	0.2	1.4	15	120	15	0.12	1.16
B	56.10	162.23	15	0.7	2.5	13	140	9	0.4	2.0
C	56.05	162.35	15	0.2	1.4	8	110	9	0.12	1.16
D	56.12	162.36	25	0.2	1.4	10	125	15	0.12	1.16
E	56.14	162.32	15	0.2	1.4	7.2	125	9	0.12	1.16
F	56.13	162.45	25	0.2	1.4	17	130	15	0.12	1.16
G	56.20	162.52	15	0.2	1.4	14	145	9	0.12	1.16
H	56.18	162.66	15	1.2	0.8	9	220	9	0.57	0.7
I	56.08	162.75	25	0.2	1.4	7	230	15	0.12	1.16
J	56.05	162.81	25	0.2	1.4	7	230	15	0.12	1.16
K	55.99	162.61	25	0.2	1.4	6.6	115	15	0.12	1.16
L	56.05	162.58	25	0.2	1.4	12	125	15	0.12	1.16
M	56.03	162.23	25	0.10	0.8	10	120	15	0.25	0.30
N	**56.06**	**162.20**	**25**	**0.08**	**0.8**	**10**	**155**	**17**	**0.25**	**0.30**

Figure 13
Examples of onland slides on the coastal slopes of the Gulf of Kamchatka (image courtesy: Google Earth)

an earthquake of moment 3×10^{27} dyn cm located in the southern part of the Ozernoy Bight or the northern Kamchatskiy Peninsula, which encompasses the ISC and ERE solutions as well as the southern part of our RE confidence ellipse.

The field of wave heights from landslide sources is known to decay with lateral distance along a beach in the near field as a result of their smaller dimension as compared to dislocations. However, this property was derived by Okal and Synolakis (2004) only in the simple case of a bathymetry with translational symmetry along the shore. We explore on Fig. 17 the possible additional influence of laterally varying bathymetry, as we note on Fig. 15 an asymmetric trend in the decay of amplitudes away from Nichiro, which is faster to the NE than to the SW. We extend our ray-tracing experiments to the case of Landslide model (N), schematized as a dipolar source consisting of a trough (T) and a hump (H), by shooting rays equally spaced at regular $4°$ degree intervals in

azimuth from each of the poles, using time steps of 20 s. Figure 17b is an interpretation of the dataset on frame (a), obtained by color-coding the density of points in (a) per $0.05° \times 0.05°$ area. Both frames show that the actual bathymetry of the bight acts to strengthen the decay of the wave in the northeast direction, towards Ust'-Kamchatsk from its maximum around Nichiro; they predict a slower decay, and thus larger amplitudes towards the SW, where however the coast quickly becomes rugged and elevated, suggesting that it was most probably uninhabited in 1923 and that any wave action would have remained unreported. This experiment provides physical insight into the general pattern of directivity of the wavefield of the preferred Landslide source (N) for the tsunami of 13 April 1923.

Another potential datum from the historical reports of the UK tsunami is the time interval of 15 min separating the two major waves at Ust'-Kamchatsk (Soloviev and Ferchev 1961), which could be
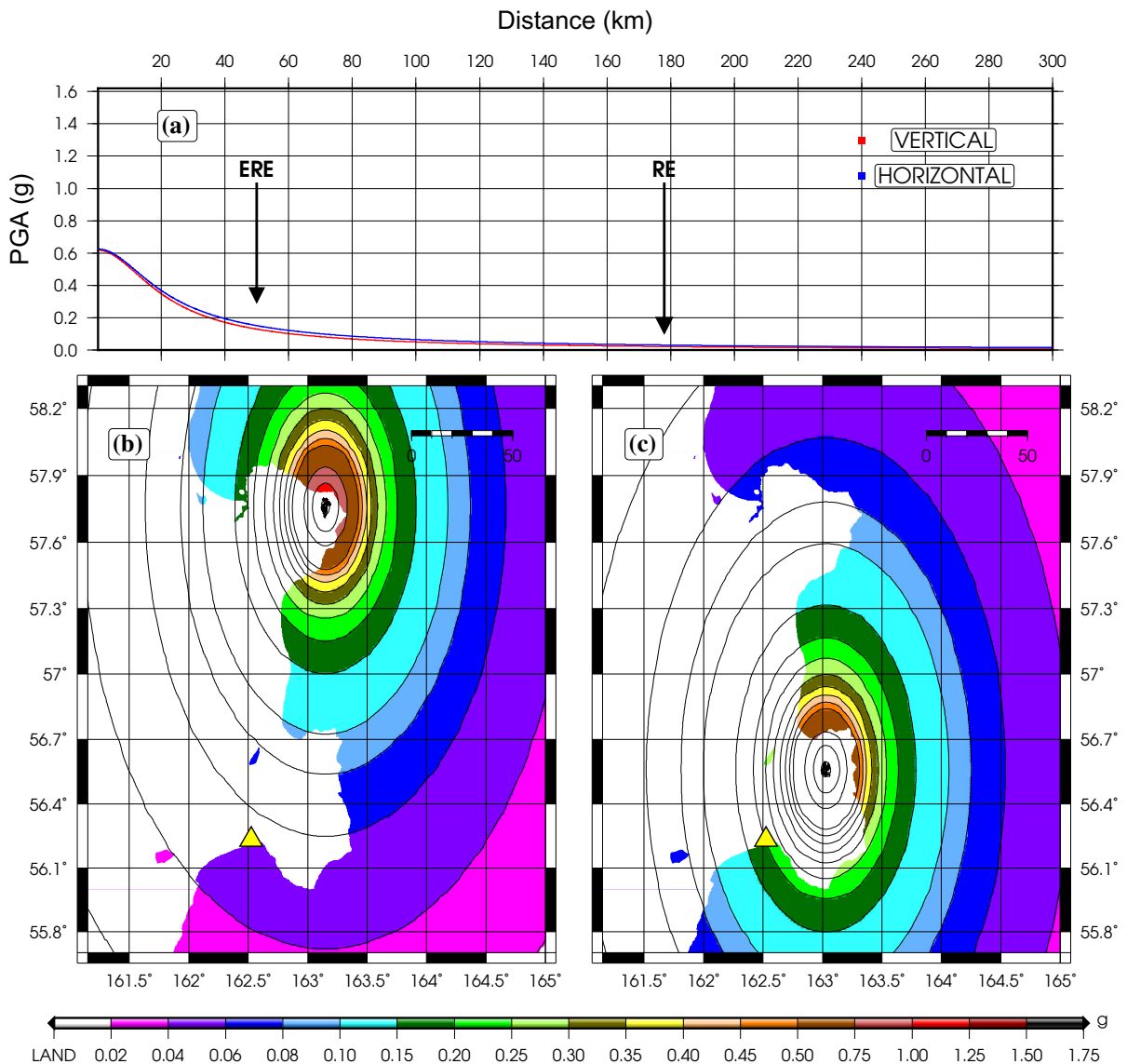
Figure 14
Calculated peak ground acceleration (PGA) at 10 Hz in units of *g* for the 13 April 1923 event, assuming a thrust mechanism with a magnitude of $M_w = 7.6$ and a focal depth of 10 km. **a** The attenuation curve showing acceleration decay with distance. Distances to the Engdahl relocation (ERE) and the relocated epicenter from this study (RE) to Ust'-Kamchatsk are depicted with arrows; **b** the PGA from the ERE epicenter; **c** the PGA from the RE epicenter. Ust'-Kamchatsk is shown with yellow triangles in **b** and **c**

interpreted as expressing the dominant period in the spectrum of the local tsunami wave. As such, it is tempting to use this observation as a further constraint on the source of the 1923 tsunami. In simple terms, the spectrum of an earthquake-generated tsunami should be controlled primarily by the dimensions of the source, principally its fault width *W*; we have verified that wavetrains simulated off

Ust'-Kamchatsk for our various earthquake scenarios have spectra peaked around 1450 and 2100 s, respectively, for the average and upper bound moments. By contrast, landslide tsunamis, emanating from spatially smaller sources, should have higher frequency spectra. However, it has long been known that tsunamis recorded at shorelines have spectra strongly affected by the natural frequencies of bights
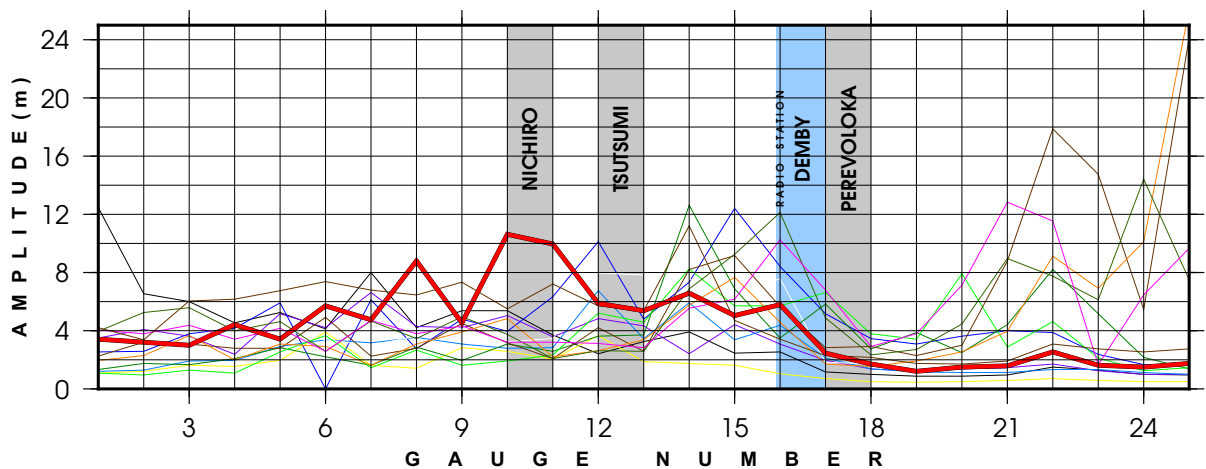
Figure 15
Tsunami heights recorded at 41 virtual gauges for the 14 landslide scenarios. The curves are color-coded to match their corresponding slides in
Fig. 12

and bays, an idea already expressed by Omori (1902). Rabinovich (1997) has shown that the resulting spectral peak of a tsunami record is a complex combination of source and receiver properties, which can be unraveled only using a sufficiently rich dataset, comprising for example the spectral properties of background noise in the absence of the tsunami signal. In this context, a single datum for what may be interpreted as a dominant period cannot provide additional constraints on the source of the tsunami. We also note that the lone available report ("Fifteen minutes after the first wave, a second wave moved in"), compiled from witness memories by Troshin and Diagilev (1926), months if not years after the fact, cannot be taken as more than an order of magnitude of the time between the two waves, and clearly lacks the precision required to be used as a scientific datum.

5. Conclusion

Our principal conclusions on the Ust'-Kamchatsk earthquake and tsunami of 13 April 1923 can be summarized as follows:

- The UK earthquake of 13 April 1923 is confirmed as an anomalously slow event, featuring a weak spectrum at short periods, and a seismic moment

increasing significantly at mantle frequencies (5 mHz). In this context, it is comparable to other "tsunami earthquakes" occurring in the aftermath of a major subduction event, such as during the 1963 Kuril and 1932 Mexican series.

- On the other hand, the majority of modern relocation efforts (ISC-GEM, E.R. Engdahl's, and our own solution) suggest that the UK earthquake did not constitute a genuine aftershock of the main event of 03 February, but rather took place north of the Kamchatka subduction zone, possibly at Cape Kamchatskiy, more probably inside the Kamchatskiy Peninsula, or even as far away as the Ozernoy Bight. The latter could also help interpret tsunami deposits identified by Bourgeois et al. (2006) at Stolbovaya Bay as dating back to between 1854 and 1956.

- The scarce dataset of available mantle wave records is difficult to reconcile with the subduction geometry of the mainshock, further suggesting that the UK earthquake is not part of a classic aftershock sequence. On their basis, the static seismic moment is estimated at 3×10^{27} dyn cm, suggesting a seismic slip on the order of 2.2 m.

- In this context, we note that the slip released during the 1971 earthquake (estimated at 2.8 m) is in excellent agreement with that predicted by plate tectonics models for the 35 years elapsed since the 1936 event (NUVEL: 7.8 cm/year in the azimuth
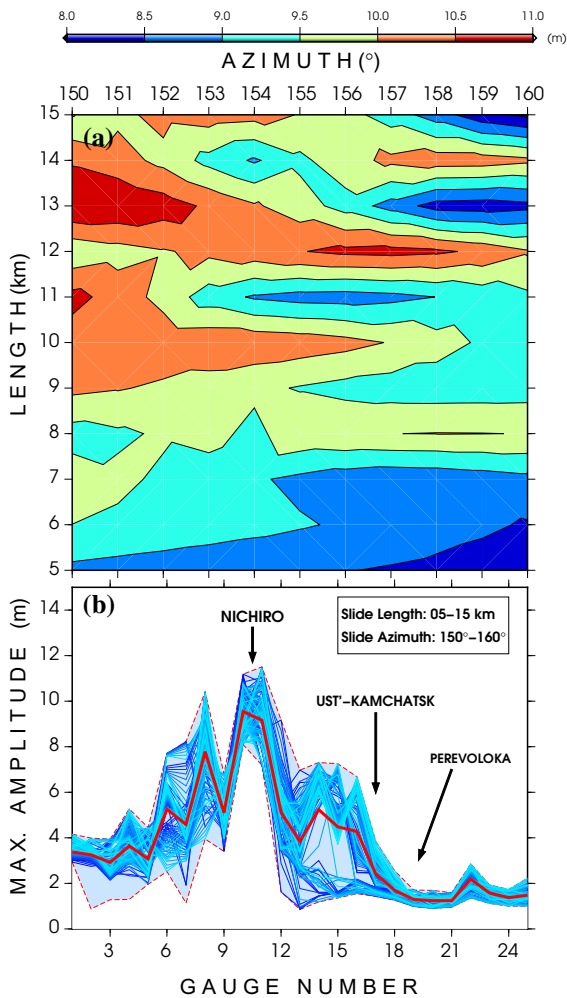
Figure 16

a Maximum calculated amplitudes at Nichiro as a function of dipole length and azimuth; **b** maximum amplitudes at the 25 virtual gauges shown in Figs. 12 and 15 while varying slide dipole length and azimuth. The red curve is connecting the average values at each gauge. The shaded area depicts the range between the maxima and minima (the red dashed curves)

- While the dataset of reported run-up values from the UK tsunami remains scant, it is characterized by very large (20 m or more) values at Nichiro, falling down to 2 m or less at Perevoloka, about 40 km away. This combination of high run-ups and peaked distribution cannot be simulated using any legitimate seismic source, especially since a rapid fall-off with distance along the beach constitutes a robust discriminant between dislocative and landslide sources (Okal and Synolakis 2004).

- While the seismic dislocation must have contributed to the tsunami, we show that it is insufficient to account for the distribution of observed amplitudes. Rather, we give a model of generation of the UK tsunami by a landslide which satisfactorily reproduces this distribution, with an acceptable offshore wave amplitude at Nichiro (12 m). The source parameters for the landslide are consistent with the known gradient field of bathymetry, with the macroseismic effects of the earthquake reported at Ust'-Kamchatsk, and with the ubiquitous presence of aerial landslides along the nearby elevated shorelines.

The present study exacerbates the strong diversity of environments and mechanisms for "tsunami earthquakes". As previously reviewed (Okal 2008; Okal and Saloor 2017), these events have generally been described as falling into two categories: "Aftershock tsunami earthquakes" (ATEs) occurring in the aftermath of mega events, and "Primary tsunami earthquakes" (PTEs) taking place as mainshocks. Typical examples of ATEs are the 20 October 1963 Kuril or 22 June 1932 Mexican earthquakes, and of PTEs the 1992 Nicaragua or 1994 and 2006 Java events.

Previous work had already pointed out diverse patterns for ATEs, with some events (e.g., Mentawai 2010) simply rupturing an extension of the plate interface upwards from the mainshock (Hill et al. 2012) while others (e.g., Kuril 1963 (20 Oct.) and 1975) would take place by stress transfer along splay faults in accretionary prisms, as originally proposed by Fukao (1979). The 1923 Kamchatka tsunami earthquake presents a variation to the latter, where the stress transfer can occur across a plate boundary, into an a priori different tectonic environment. In
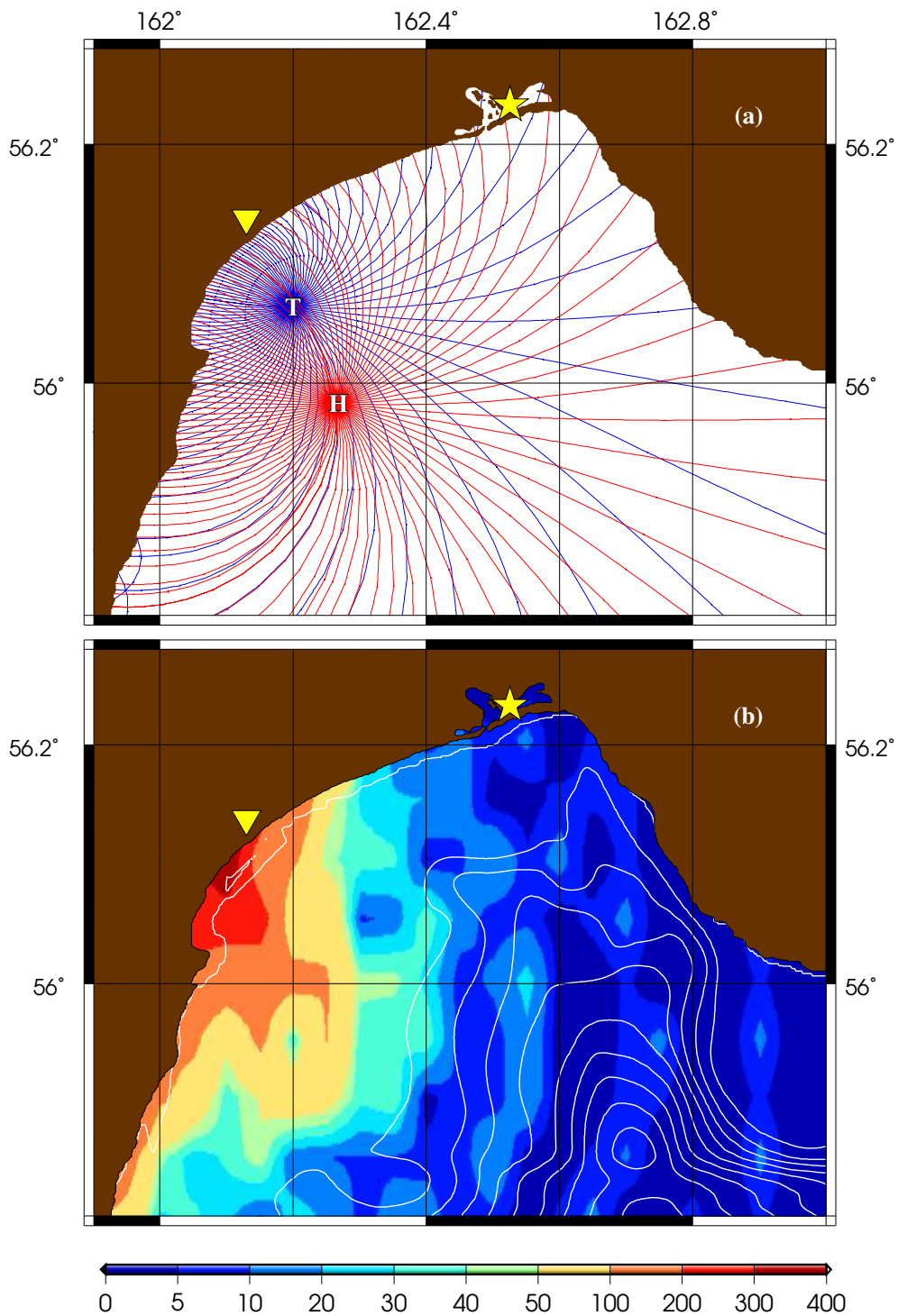
311° (DeMets et al. 1990); REVEL: 7.5 cm/year in the azimuth 306° (Sella et al. 2002)), while the slip accumulated between the previous tsunami documented in the Commander Islands in 1849 (Soloviev and Ferchev 1961) and 1936, would amount to 6.5–6.8 m, a figure intermediate between the estimated slips of the 1917–1936 doublet (5.2 m) and of a possible 1917–1923–1936 trio (7.4 m). On this basis, it is not possible to exclude the common location of the 1917, 1936 and 1971 events as an epicenter for the UK event.

Figure 17
a Ray-tracing of the slide dipole. Blue and red lines show rays propagating, respectively, from the trough (T) and the hump (H) of the dipole;
b number of ray points per $0.05° \times 0.05°$ area calculated from (**a**). The yellow stars and inverted triangles represent Ust'-Kamchatsk and Nichiro, respectively

addition, our study provides new evidence for the role of underwater landslides, triggered by earthquakes, in the generation of tsunamis with catastrophic amplitudes on nearby shorelines. In this respect, the UK event is comparable to the great 1946 Aleutian one, which similarly combined a very slow seismic source and an underwater landslide, even though that earthquake would qualify as a PTE, and featured a much larger seismic moment.

Finally, we note that the reported maximum run-up (at least 20 m) and inundation (7 km into the mouth of the Kamchatka River) were larger than measured along a similarly flat shoreline during the 1998 Papua New Guinea tsunami (15 m and at most 1 km (Synolakis et al. 2002)); thus a comparable societal disaster was avoided only thanks to the sparse population of the affected area. Considering the fundamentally non-linear nature of the sliding process, and our obviously limited knowledge of the relevant population of precarious masses with potential for destabilization on the sea floor, the 1923 Ust'-Kamchatsk earthquake casts an ominous augury in terms of seismic hazard for coastal communities in seismic areas worldwide.

Acknowledgements

REFERENCES

Aki, K., & Richards, P. G. (2002). *Quantitative seismology*. University Science Books.

Ambraseys, N. (1991). The Rukwa earthquake of 13 December 1910 in East Africa. *Terra Nova*, *3*(2), 202–211.

Anonymous. (2001). *Province of Kamchatka map*. Moscow: Federal Service of Geodesy and Geography of Russia.

Bell, R., Holden, C., Power, W., Wang, X., & Downes, G. (2014). Hikurangi margin tsunami earthquake generated by slow seismic rupture over a subducted seamount. *Earth and Planetary Science Letters*, *397*, 1–9.

Borisov, V. I. (2002). Forgotten Tragedy, www.kamchatsky-krai.ru/geography/article/borisov.htm, Accessed on October 23, 2017 [in Russian].

Bourgeois, J., & Pinegina, T. K. (2017). 1997 Kronotsky earthquake and tsunami and their predecessors, Kamchatka, Russia. *Natural Hazards and Earth System Sciences Discussions* (submitted).

Bourgeois, J., Pinegina, T. K., Ponomareva, V., & Zaretskaia, N. (2006). Holocene tsunamis in the southwestern Bering Sea, Russian Far East, and their tectonic implications. *Geological Society of America Bulletin*, *118*(3–4), 449–463.

Brunsden, D., & Prior, D. B. (1984). *Slope instability*. New York: Wiley.

Campbell, K. W., & Bozorgnia, Y. (2003). Updated near-source ground-motion (attenuation) relations for the horizontal and vertical components of peak ground acceleration and acceleration response spectra. *Bulletin of the Seismological Society of America*, *93*(1), 314–331.

Cormier, V. F. (1975). Tectonics near the junction of the Aleutian and Kuril-Kamchatka arcs and a mechanism for middle Tertiary magmatism in the Kamchatka basin. *Geological Society of America Bulletin*, *86*(4), 443–453.

Courant, R., Friedrichs, K., & Lewy, H. (1928). Über die partiellen Differenzengleichungen der mathematischen Physik. *Mathematische Annalen*, *100*(1), 32–74.

Daughton, T. M. (1990). *Focal mechanism of the 22 November 1969 Kamchatka earthquake from teleseismic waveform analysis*. Honors Thesis, Colorado College, Colorado Springs. 70 pp.

DeMets, C., Gordon, R. G., Argus, D., & Stein, S. (1990). Current plate motions. *Geophysical Journal International*, *101*(2), 425–478.

Dziewonski, A., Chou, T.-A., & Woodhouse, J. (1981). Determination of earthquake source parameters from waveform data for studies of global and regional seismicity. *Journal of Geophysical Research: Solid Earth*, *86*(B4), 2825–2852.

Ebel, J. E., & Chambers, D. W. (2016). Using the locations of $M \geq 4$ earthquakes to delineate the extents of the ruptures of past major earthquakes. *Geophysical Journal International*, *207*(2), 862–875.

Ekström, G., Nettles, M., & Dziewoński, A. (2012). The global CMT project 2004–2010: Centroid-moment tensors for 13,017 earthquakes. *Physics of the Earth and Planetary Interiors*, *200*, 1–9.

Engdahl, E. R., & Villaseñor, A. (2002). Global seismicity: 1900–1999.

Fedotov, C., Gusev, A., Zobin, B., Kondratienko, A., & Chepkynas, K. (1973). The Ozernovskiy earthquake and tsunami of 22 (23) November 1969. *Earthquakes in the USSR in the year 1969*, 195–208. [in Russian].

Fisher, R., Jantsch, M., & Comer, R. (1982). General Bathymetric Chart of the Oceans (GEBCO).

Fryer, G. J., & Watts, P. (2001). Motion of the Ugamak slide, probable source of the tsunami of 1 April 1946. In *Proceedings of the International Tsunami Symposium* (pp. 683–694).

Fukao, Y. (1979). Tsunami earthquakes and subduction processes near deep-sea trenches. *Journal of Geophysical Research: Solid Earth*, *84*(B5), 2303–2314.

Geller, R. J. (1976). Scaling relations for earthquake source parameters and magnitudes. *Bulletin of the Seismological Society of America*, *66*(5), 1501–1523.

Gorin, S., & Chebanova, V. (2011). Salinization-related transformation of hydrological regime and benthos in the Nerpichye and Kultuchnoe Lakes, at the Kamchatka River estuary. In *V.V. Levandinov Memorial Lectures* (pp. 119–128). Vladivostok: Russian Academy of Sciences [in Russian].

Gusev, A. A. (2004). Schematic map of the source zones of large Kamchatka earthquakes of the instrumental epoch. In *Complex seismological and geophysical investigations of Kamchatka* (pp. 75–80). Petropavlovsk–Kamchatsky. [in Russian].

Gusev, A. A., Zobin, V. M., Kondratenko, A. M., & Shumilina, L. S. (1975). The earthquake of Ust'-Kamchatsk, 15 XII. *Earthquakes in the USSR in the year 1971* (pp. 172–184) [in Russian].

Gutenberg, B., & Richter, C. F. (1954). *Seismicity of the Earth and associated phenomena*. Princeton, NJ: Princeton Univ. Press.

Hill, E. M., Borrero, J. C., Huang, Z., Qiu, Q., Banerjee, P., Natawidjaja, D. H., et al. (2012). The 2010 $M_w = 7.8$ Mentawai earthquake: Very shallow source of a rare tsunami earthquake determined from tsunami field survey and near-field GPS data. *Journal of Geophysical Research: Solid Earth*, *117*, B06402.

Hoffmann, G., Al-Yahyai, S., Naeem, G., Kociok, M., & Grützner, C. (2014). An Indian Ocean tsunami triggered remotely by an onshore earthquake in Balochistan, Pakistan. *Geology*, *42*(10), 883–886.

Jaggar, T. (1930). *Volcano letter*, *274*, 1–4.

Jobert, N., & Jobert, G. (1983). An application of ray theory to the propagation of waves along a laterally heterogeneous spherical surface. *Geophysical Research Letters*, *10*(12), 1148–1151.

Kanamori, H. (1972). Mechanism of tsunami earthquakes. *Physics of the Earth and Planetary Interiors*, *6*(5), 346–359.

Kanamori, H. (1977). The energy release in great earthquakes. *Journal of Geophysical Research*, *82*(20), 2981–2987.

Kanamori, H. (1985). Non-double-couple seismic source. In *Proc: XXIIIrd Gen. Assemb. Intl. Assoc. Seismol. Phys. Earth Inter* (p. 425)

Kawata, Y., Benson, B. C., Borrero, J. C., Borrero, J. L., Davies, H. L., Lange, W. P., et al. (1999). Tsunami in Papua New Guinea was as intense as first thought. *Eos, Transactions American Geophysical Union*, *80*(9), 101–105.

Keefer, D. K. (1984). Landslides caused by earthquakes. *Geological Society of America Bulletin*, *95*(4), 406–421.

Kuksina, L., & Chalov, S. (2012). The suspended sediment discharge of the rivers running along territories of contemporary volcanism in Kamchatka. *Geography and Natural Resources*, *33*(1), 67–73.

López, A. M., & Okal, E. A. (2006). A seismological reassessment of the source of the 1946 Aleutian 'tsunami' earthquake. *Geophysical Journal International*, *165*(3), 835–849.

Mansinha, L., & Smylie, D. (1971). The displacement fields of inclined faults. *Bulletin of the Seismological Society of America*, *61*(5), 1433–1440.

Martin, M. E., Weiss, R., Bourgeois, J., Pinegina, T. K., Houston, H., & Titov, V. V. (2008). Combining constraints from tsunami modeling and sedimentology to untangle the 1969 Ozernoi and 1971 Kamchatskii tsunamis. *Geophysical Research Letters*, *35*, L01610.

Meniaĭlov, A. A. (1946). Tsunamis in the Ust'-Kamchatsk region. *Bull. Kamchatka Volcanol. Stn.* (Vol. 12) [in Russian].

Minoura, K., Gusiakov, V., Kurbatov, A., Takeuti, S., Svendsen, J., Bondevik, S., et al. (1996). Tsunami sedimentation associated with the 1923 Kamchatka earthquake. *Sedimentary Geology*, *106*(1–2), 145–154.

Newman, A. V., & Okal, E. A. (1998). Teleseismic estimates of radiated seismic energy: The E/M_0 discriminant for tsunami earthquakes. *Journal of Geophysical Research: Solid Earth*, *103*(B11), 26885–26898.

Okal, E. (2008). The excitation of tsunamis by earthquakes. In E. Bernard & A. Robinson (Eds.) *The Sea: Ideas and observations on progress in the study of the seas* (pp. 137–177). Cambridge: Harvard Univ. Press.

Okal, E. A. (1992). Use of the mantle magnitude M_m for the reassessment of the moment of historical earthquakes. *Pure and Applied Geophysics*, *139*(1), 17–57.

Okal, E. A. (2003). Normal mode energetics for far-field tsunamis generated by dislocations and landslides. *Pure and Applied Geophysics*, *160*(10), 2189–2221.

Okal, E. A. (2011). Tsunamigenic earthquakes: past and present milestones. *Pure and Applied Geophysics*, *168*(6–7), 969–995.

Okal, E. A., & Borrero, J. C. (2011). The 'tsunami earthquake' of 1932 June 22 in Manzanillo, Mexico: seismological study and tsunami simulations. *Geophysical Journal International*, *187*(3), 1443–1459.

Okal, E. A., & Saloor, N. (2017). Historical tsunami earthquakes in the Southwest Pacific: An extension to $\Delta > 80°$ of the energy-to-moment parameter Θ. *Geophysical Journal International*, *210*(2), 852–873.

Okal, E. A., & Synolakis, C. E. (2004). Source discriminants for near-field tsunamis. *Geophysical Journal International*, *158*(3), 899–912.

Okal, E. A., & Talandier, J. (1986). T-wave duration, magnitudes and seismic moment of an earthquake—Application to tsunami warning. *Journal of Physics of the Earth*, *34*(1), 19–42.

Okal, E. A., & Talandier, J. (1989). M_m: A variable-period mantle magnitude. *Journal of Geophysical Research: Solid Earth*, *94*(B4), 4169–4193.

Okal, E. A., Plafker, G., Synolakis, C. E., & Borrero, J. C. (2003). Near-field survey of the 1946 Aleutian tsunami on Unimak and Sanak Islands. *Bulletin of the Seismological Society of America*, *93*(3), 1226–1234.

Okal, E. A., Fritz, H. M., Raad, P. E., Synolakis, C., Al-Shijbi, Y., & Al-Saifi, M. (2006a). Oman field survey after the December 2004 Indian Ocean tsunami. *Earthquake Spectra*, *22*(S3), 203–218.

Okal, E. A., Fritz, H. M., Raveloson, R., Joelson, G., Pančošková, P., & Rambolamanana, G. (2006b). Madagascar field survey after the December 2004 Indian Ocean tsunami. *Earthquake Spectra*, *22*(S3), 263–283.

Okal, E. A., Synolakis, C. E., Uslu, B., Kalligeris, N., & Voukouvalas, E. (2009). The 1956 earthquake and tsunami in Amorgos, Greece. *Geophysical Journal International*, *178*(3), 1533–1554.

Okal, E. A., Visser, J. N., & de Beer, C. H. (2014). The Dwarskersbos, South Africa local tsunami of August 27, 1969: Field survey and simulation as a meteorological event. *Natural Hazards*, *74*(1), 251–268.

Omori, F. (1902). On tsunamis around Japan. *Rep. Imper. Earthq. Comm.*, *34*, 5–79 [in Japanese].

Polet, J., & Kanamori, H. (2000). Shallow subduction zone earthquakes and their tsunamigenic potential. *Geophysical Journal International*, *142*(3), 684–702.

Prior, D. B., Bornhold, B. D., Coleman, J. M., & Bryant, W. R. (1982). Morphology of a submarine slide, Kitimat Arm, British Columbia. *Geology*, *10*(11), 588–592.

Rabinovich, A. B. (1997). Spectral analysis of tsunami waves: Separation of source and topography effects. *Journal of Geophysical Research: Oceans*, *102*(C6), 12663–12676.

Salaree, A., & Okal, E. A. (2015). Field survey and modelling of the Caspian Sea tsunami of 1990 June 20. *Geophysical Journal International*, *201*(2), 621–639.

Satake, K. (1988). Effects of bathymetry on tsunami propagation: Application of ray tracing to tsunamis. *Pure and Applied Geophysics*, *126*(1), 27–36.

Sella, G. F., Dixon, T. H., & Mao, A. (2002). REVEL: A model for recent plate velocities from space geodesy. *Journal of Geophysical Research: Solid Earth*, *107*(2081).

Shuto, N., Suzuki, T., & Hasegawa, K. (1986). A study of numerical techniques on the tsunami propagation and run-up. *Science of Tsunami Hazard*, *4*, 111–124.

Skempton, A. (1953). Soil mechanics in relation to geology. *Proceedings of the Yorkshire Geological Society*, *29*(1), 33–62.

Soloviev, S., Go, C. N., & Kim, K. S. (1986). Catalog of tsunamis in the Pacific, 1969–1982, *Moscow: USSR Academy of Sciences, Soviet Geophysical Committee*, [in English; translation: Amerind Publishing Co., New Delhi, 1998].

Soloviev, S., Campos-Romero, M., & Plink, N. (1992). Orléansville tsunami of 1954 and El Asnam tsunami of 1980 in the Alboran Sea (Southwestern Mediterranean Sea). *Izvestiya Earth Phys*, *28*(9), 739–760.

Soloviev, S. L., & Ferchev, M. D. (1961). Summary of data on tsunamis in the USSR, Bull. Council Seism. Acad. *USSR*, *9*, 23–55.

Stauder, W., & Mualchin, L. (1976). Fault motion in the larger earthquakes of the Kurile-Kamchatka Arc and of the Kurile-Hokkaido corner. *Journal of Geophysical Research*, *81*(2), 297–308.

Storchak, D., Di Giacomo, D., Engdahl, E., Harris, J., Bondár, I., Lee, W., et al. (2015). The ISC-GEM global instrumental earthquake catalogue (1900–2009): Introduction. *Physics of the Earth and Planetary Interiors*, *239*, 48–63.

Synolakis, C., Bernard, E., Titov, V., Kânoğlu, U., & González, F. (2008). Validation and verification of tsunami numerical models. *Pure and Applied Geophysics*, *165*(11–12), 2197–2228.

Synolakis, C. E., Bardet, J.-P., Borrero, J. C., Davies, H. L., Okal, E. A., Silver, E. A., Sweet, S., & Tappin, D. R. (2002). The slump origin of the 1998 Papua New Guinea tsunami. *Proceedings of the Royal Society of London, Series A*, *458*, 763–789.

Tanioka, Y., Ruff, L., & Satake, K. (1997). What controls the lateral variation of large earthquake occurrence along the Japan Trench? *Island Arc*, *6*(3), 261–266.

The Los Angeles Times. (1923). *15 April 1923*.

Titov, V. & González, F. (1997). *Implementation and Testing of the Method of Splitting Tsunami (MOST) Model*, US Department of Commerce, National Oceanic and Atmospheric Administration, Environmental Research Laboratories, Pacific Marine Environmental Laboratory.

Titov, V., Kânoğlu, U., & Synolakis, C. (2016). Development of MOST for real-time tsunami forecasting. *Journal of Waterway, Port, Coast and Oceanic Engineering*, *142*, 03116004-1–03116004-16.

Titov, V. V., & Synolakis, C. E. (1995). Modeling of breaking and nonbreaking long-wave evolution and runup using VTCS-2. *Journal of Waterway, Port, Coastal, and Ocean Engineering*, *121*(6), 308–316.

Titov, V. V., & Synolakis, C. E. (1997). Extreme inundation flows during the Hokkaido-Nansei-Oki tsunami. *Geophysical Research Letters*, *24*(11), 1315–1318.

Titov, V. V., & Synolakis, C. E. (1998). Numerical modeling of tidal wave run-up. *Journal of Waterway, Port, Coastal, and Ocean Engineering*, *124*(4), 157–171.

Troshin, A. N., & Diagilev, G. A. (1926). *The Ust' Kamchatsk earthquake of April 13, 1923*. Library Institute Physics Earth, USSR Academy of Sciences, Moscow [in Russian].

Utsu, T. (1970). Aftershocks and earthquake statistics (1): Some parameters which characterize an aftershock sequence and their interrelations. *Journal of the Faculty of Science, Hokkaido University. Series 7, Geophysics*, *3*(3), 129–195.

von Huene, R., Kirby, S., Miller, J., & Dartnell, P. (2014). The destructive 1946 Unimak near-field tsunami: New evidence for a submarine slide source from reprocessed marine geophysical data. *Geophysical Research Letters*, *41*(19), 6811–6818.

Wald, D. J., Quitoriano, V., Heaton, T. H., & Kanamori, H. (1999). Relationships between peak ground acceleration, peak ground velocity, and modified Mercalli intensity in California. *Earthquake Spectra*, *15*(3), 557–564.

Wessel, P., & Smith, W. H. (1991). Free software helps map and display data, *Eos, Transactions American Geophysical Union*, *72*(41), 441 and 445–446.

Woods, M. T., & Okal, E. A. (1987). Effect of variable bathymetry on the amplitude of teleseismic tsunamis: A ray-tracing experiment. *Geophysical Research Letters*, *14*(7), 765–768.

Wysession, M. E., Okal, E. A., & Miller, K. L. (1991). Intraplate seismicity of the Pacific Basin, 1913–1988. *Pure and Applied Geophysics*, *135*(2), 261–359.

Zayakin, Y., & Luchinina, A. (1987). *Catalogue of Tsunamis on Kamchatka*. Obninsk: VNIIGMI-MTSD. [in Russian].